Unified Emergent Condensate Superfluid Medium Cosmology: A Superfluid Framework for Gravity, Redshift, and Structure Formation without Dark Matter or Expansion

Adam Sheldrick

Independent Researcher

January 31, 2026

Preprint / Working Draft (v1.0)

Several figures in this framework manuscript are schematic placeholders intended to illustrate concepts. Quantitative plots and full numerical validations are provided in companion and follow-up papers.

Abstract

We present a unified theoretical framework in which gravity, cosmological redshift, galaxy rotation curves, black hole horizons, and large-scale structure arise from the dynamics of a single physical medium: a compressible, superfluid-like medium field. The model requires no dark matter, no dark energy, and no expanding spacetime. Instead, gravitational phenomena emerge from gradients in the effective propagation speed of disturbances in the medium, while redshift is produced by wave propagation through large-scale background flows. Galaxy rotation curves arise from stabilized ECSM vortices, yielding flat velocity profiles and the baryonic Tully–Fisher relation. Black holes correspond to regions where the inward Condensate Response Flow

reaches the local effective wave speed, forming acoustic horizons without singularities. We develop the field equations, derive the effective metric, present the cosmological implications, and provide observationally testable predictions, including modifications to lensing, non-expanding redshift drift, horizon echoes, and CMB acoustic structure. This work establishes a coherent, falsifiable alternative to general relativity and ΛCDM.

1 Introduction

ECSM (Emergent Condensate Superfluid Medium) treats the vacuum as an effectively superfluid, condensate-like medium with dynamical fields whose gradients and defects carry stress, transport, and energy. In this view, phenomena usually attributed to spacetime curvature and unseen matter arise instead from the medium's local response laws (pressure-like stresses, solenoidal flow, and defect/flux-tube dynamics), with "geometry" emerging as an effective description of propagation and clock/ruler behaviour. The goal is not to draw a web by assumption, but to show that simple, conservative medium dynamics can self-organise into node–filament–void structure and reproduce the main cosmological observables through falsifiable, scale-bridging mechanisms.

Modern cosmology relies on several unobserved components—dark matter, dark energy, inflation—in order to reconcile theory with observation. General relativity provides an elegant geometric interpretation of gravity, yet the inferred matter content of the universe is dominated by invisible and unexplained substances [1, 2]. Furthermore, the interpretation of cosmological redshift as a consequence of metric expansion leads to several conceptual issues, including horizon problems, fine-tuning, and unrealistically smooth early-universe conditions.

In this work we pursue a different approach: the emergence of gravitational and cosmological phenomena from the dynamics of a single physical medium, the ECSM. While historically abandoned, the concept of a physical medium proved remarkably successful in condensed matter analogues of black holes, horizon physics, and effective spacetime metrics. We develop a model in which the ECSM is a compressible, irrotational superfluid with density $n(\mathbf{x}, t)$ and phase $\theta(\mathbf{x}, t)$, whose excitations propagate with an effective speed $c_{\text{eff}}(n)$ that varies with density. Gravity emerges from spatial

variations in c_{eff}, redshift from large-scale flows $v(\mathbf{x})$, and galaxy rotation curves from long-lived vortex structures.

This paper presents the full theoretical development, observational consequences, and falsifiable predictions of this framework.

Interpretive Convention and Terminology

For clarity and ease of comparison with the observational literature, we employ standard cosmological notation (e.g. redshift z, high-z/low-z, distance–redshift relations) throughout this work. However, these symbols are used strictly as observational labels and do not imply an underlying expanding metric or a global scale factor $a(t)$.

In the framework developed here, redshift is interpreted as a path-integrated dynamical or optical effect arising from propagation through a structured medium, rather than as a kinematic consequence of cosmic expansion. Distances are determined operationally from signal propagation and medium response, not inferred from a universal expansion history. Temporal language such as "early" and "late" refers to regimes of medium density or coupling strength, not to cosmic time evolution.

A summary of correspondences is provided below:

Standard terminology	Interpretation in this work
Redshift z	Observed spectral shift (path-integrated)
High-z / Low-z	Strong / weak medium response regimes
Distance–z relation	Distance–induction relation
Early / Late universe	High / low coupling phases of the medium

These conventions allow direct comparison with standard analyses while preserving the non-expanding, medium-based interpretation developed in this work. Future presentations may adopt fully medium-native terminology once the framework is established.

1.1 Canonical definition of redshift in a state-dependent medium

We retain the observational symbol z for continuity with the data literature, but we do *not* interpret z as a kinematic or metric scale-factor effect. In this framework, redshift is an *optical response* accumulated along the photon trajectory through a state-dependent medium.

Operational definition. Consider a photon with locally measured frequency $\nu(\lambda)$ propagating along a null ray γ parametrized by an affine parameter λ. We define the observed redshift between emission at $\lambda = \lambda_{\rm e}$ and observation at $\lambda = \lambda_{\rm o}$ by

$$1 + z \;\equiv\; \frac{\nu_{\rm e}}{\nu_{\rm o}} \;=\; \exp\!\left(\int_{\lambda_{\rm e}}^{\lambda_{\rm o}} \mathcal{I}[\chi(x), \nabla\chi(x), u^{\mu}(x), \ldots]\, \mathrm{d}\lambda\right), \tag{1}$$

where $\chi(x)$ is a medium state variable (e.g. an order parameter, coherence, or density proxy), $u^{\mu}(x)$ is a possible Condensate Response Flow field, and $\mathcal{I}$ is a scalar *induction rate* functional with dimensions of inverse affine length. Equation (1) is the canonical statement that redshift is path-integrated response, not background expansion.

Differential form. Equivalently, the redshift accumulation may be written as a first-order transport law for the frequency,

$$\frac{\mathrm{d}}{\mathrm{d}\lambda} \ln \nu(\lambda) \;=\; -\,\mathcal{I}[\chi, \nabla\chi, u^{\mu}, \ldots]\,, \qquad \Rightarrow \qquad 1+z = \exp\!\left(-\int_{\lambda_{\rm e}}^{\lambda_{\rm o}} \frac{\mathrm{d}}{\mathrm{d}\lambda} \ln \nu \, \mathrm{d}\lambda\right), \tag{2}$$

so that any nontrivial z arises from a nonzero $\mathcal{I}$ along the ray.

Minimal "state-driven" choice. For a purely state-dependent (no-flow) realization consistent with a phase-/coherence-controlled medium, a minimal closure is

$$\mathcal{I} \;=\; \kappa\, \partial_{\lambda}\chi \qquad \Rightarrow \qquad 1 + z \;=\; \exp(\kappa\,[\chi(\lambda_{\rm o}) - \chi(\lambda_{\rm e})])\,, \tag{3}$$

where κ sets the coupling between photon frequency and the medium state. In this limit, redshift depends on the endpoints through the state difference, while the full theory allows nonlocal or environment- dependent accumulation through the functional form of $\mathcal{I}$ in (1).

Distance is not assumed from redshift. Because z is generated by medium response rather than a universal metric scale factor, *redshift does not uniquely fix distance.* Distance measures (e.g. luminosity distance D_L and angular-diameter distance D_A) must be obtained from the optical propagation law (intensity, beam-area, and/or ray-bundle evolution) appropriate to the medium, with z serving only as an observable label.

Notation and "expansion language." Where convenient, one may introduce an *effective* kinematic mapping (e.g. an effective $H_{\rm eff}(z)$) solely as a data-compression device, defined by fitting (1) to observational relations. Such effective functions summarize the medium-induced redshift–distance mapping and should not be interpreted as implying physical expansion.

2 Consistency Requirements for a Medium-Based Gravitational Theory

2.1 No-drag regime and the Landau criterion

A common objection to any medium-based model is the expectation of vacuum drag: objects moving through a medium should dissipate energy into excitations of that medium. In a superfluid-like ground state, however, dissipation-free motion is kinematically protected by the Landau criterion.

For a medium with excitation spectrum $E(p)$, emission of excitations by an object moving at speed v is possible only if energy–momentum conservation admits modes satisfying $E(p) - vp \leq 0$. Landau showed that dissipation is forbidden whenever

$$v < v_c, \qquad v_c \equiv \min_{p>0} \left(\frac{E(p)}{p} \right). \tag{4}$$

In the condensate toy model used here, the low-energy spectrum is phonon-like, $E(p) \simeq c_s p$ with higher-order corrections suppressed by a large scale Λ. Consequently,

$$\frac{E(p)}{p} \simeq c_s + \mathcal{O}(p^2), \tag{5}$$

and the minimum occurs as $p \to 0$, yielding a critical velocity $v_c = c_s$. Motion below this threshold cannot radiate excitations and is therefore non-dissipative, providing a natural explanation for the empirical absence of vacuum friction in the low-energy regime.

2.2 Universal coupling and emergence of the equivalence principle

A central requirement of any medium-based framework is consistency with the empirical universality of free fall. In the present approach, this univer-

sality is realized by treating gravity as an effective low-energy geometry $g^{\rm eff}_{\mu\nu}$ arising from coarse-grained variables (density and flow). The leading matter dynamics are assumed to be minimally coupled to the same effective metric for all species,

$$S_{\rm matter} = \sum_i \int d^4x \, \sqrt{-g_{\rm eff}} \, \mathcal{L}_i\big(\chi_i, \nabla^{\rm eff}\chi_i; g^{\rm eff}_{\mu\nu}\big) \; + \; \Delta S_{\rm nonuniv}. \tag{6}$$

In the geometric-optics limit, wave packets follow the same effective geodesics of $g^{\rm eff}_{\mu\nu}$ independent of composition, reproducing the equivalence principle.

Possible composition-dependent effects reside in higher-order, non-universal operators suppressed by a large scale Λ, $\Delta S_{\rm nonuniv} \sim \sum_i (c_i/\Lambda^n) \int d^4x \sqrt{-g_{\rm eff}}\, \mathcal{O}_i$, implying equivalence-violating effects scaling as $\eta \sim (E/\Lambda)^n$. Thus universality is recovered automatically at low energies while allowing controlled, testable deviations in extreme regimes.

2.3 Accelerated motion and radiation

The Landau criterion forbids dissipation for uniform motion below the critical velocity, but it does not forbid radiation from non-uniform motion. Acceleration introduces time-dependent forcing that can excite propagating modes of the medium, analogous to electromagnetic radiation from accelerating charges.

At the effective level, collective perturbations of the ECSM may be represented by a field ϕ obeying a wave equation on the emergent geometry,

$$\Box_{\rm eff}\, \phi = J(t, \mathbf{x}), \tag{7}$$

where J encodes disturbances produced by accelerated or time-varying mass distributions. Outgoing-wave solutions carry energy, with far-field flux scaling schematically as $P \propto \int d\Omega \, \langle (\partial_t \phi)^2 \rangle$. Thus, while steady inertial motion is non-dissipative in the superfluid ground state, accelerated motion can radiate energy into propagating medium modes.

In the limit where the effective description reproduces General Relativity, the dominant radiation is expected to arise from time-varying multipole moments, mirroring the quadrupole character of gravitational-wave emission. Quantitative matching of radiation amplitudes and propagation speed provides a direct route to constrain the medium parameters and test the framework against existing gravitational-wave observations.

3 Emergent Geometry from a Condensate-Like superfluid medium

In this section we show how an effective spacetime geometry arises as a low-energy, coarse-grained description of a condensate-like superfluid medium. Rather than postulating a metric from the outset, the geometric structure emerges kinematically from the propagation of linear excitations on an inhomogeneous and possibly flowing background medium. This construction follows the logic of analogue gravity, where the characteristics of wave equations define an effective metric governing causal structure. We derive this metric explicitly from the hydrodynamic equations of the ECSM, establish its weak-field limit, and identify the conditions under which it reproduces Newtonian gravity and relativistic light propagation.

3.1 Effective metric from condensate hydrodynamics (acoustic geometry)

We model the ECSM as a condensate order parameter $\Psi = \sqrt{n}\, e^{i\theta}$ with background density $n_0(\mathbf{x}, t)$ and phase $\theta_0(\mathbf{x}, t)$. The associated flow velocity is $\mathbf{v}_0 = (\hbar/m)\nabla\theta_0$, and the local sound speed is $c_s^2 = (g/m)\, n_0$. In the hydrodynamic regime (neglecting quantum-pressure terms), linear perturbations δn, $\delta\theta$ satisfy the linearized continuity equation together with a Bernoulli relation, $\delta n = -(n_0/c_s^2)\big[\partial_t \delta\theta + \mathbf{v}_0 \cdot \nabla\delta\theta\big]$. Eliminating δn yields a wave equation for $\delta\theta$ of the form

$$\partial_\mu (f^{\mu\nu}\partial_\nu \delta\theta) = 0, \tag{8}$$

with

$$f^{\mu\nu} = \frac{n_0}{c_s^2}\begin{pmatrix} -1 & -v_0^j \\ -v_0^i & c_s^2\delta^{ij} - v_0^i v_0^j \end{pmatrix}. \tag{9}$$

This can be written in curved-spacetime form, $(1/\sqrt{-g})\partial_\mu(\sqrt{-g}\, g_{\text{eff}}^{\mu\nu}\partial_\nu\delta\theta) = 0$, allowing identification (up to a conformal factor) of an effective metric determined by the background medium:

$$g_{\mu\nu}^{\text{eff}} = \frac{n_0}{c_s}\begin{pmatrix} -(c_s^2 - \mathbf{v}_0^2) & -v_{0j} \\ -v_{0i} & \delta_{ij} \end{pmatrix}, \qquad g_{\text{eff}}^{\mu\nu} = \frac{1}{n_0 c_s}\begin{pmatrix} -1 & -v_0^j \\ -v_0^i & c_s^2\delta^{ij} - v_0^i v_0^j \end{pmatrix}. \tag{10}$$

In the geometric-acoustics limit, wavefronts and rays propagate along null curves of $g_{\mu\nu}^{\text{eff}}$, so spatial gradients and flows in the medium naturally induce an effective curved geometry for excitations.

3.2 Weak-field limit and recovery of Newtonian dynamics

To make contact with classical gravity, we consider the simplest case of a stationary background with negligible bulk flow, $\mathbf{v}_0 = 0$, and allow only slow spatial variation of the medium state through $c_s(\mathbf{x})$ and the conformal prefactor. In this limit the effective metric derived above reduces (up to an overall conformal factor) to

$$ds^2_{\text{eff}} \propto -c_s^2(\mathbf{x})\, dt^2 + d\mathbf{x}^2. \tag{11}$$

We now parameterize weak departures from a homogeneous background by writing

$$c_s^2(\mathbf{x}) = c_0^2 \left[1 + \frac{2\Phi(\mathbf{x})}{c_0^2}\right], \qquad \left|\frac{\Phi}{c_0^2}\right| \ll 1, \tag{12}$$

where c_0 is the asymptotic propagation speed and $\Phi(\mathbf{x})$ defines an effective gravitational potential.

In the geometric-optics (ray) limit, trajectories follow null curves of the effective metric. For slowly moving massive probes, one may equivalently consider the nonrelativistic limit of the effective action,

$$S \simeq -m \int dt\, c_s(\mathbf{x}) \sqrt{1 - \frac{\dot{\mathbf{x}}^2}{c_s^2(\mathbf{x})}} \;\approx\; \int dt \left[\frac{m}{2}\dot{\mathbf{x}}^2 - m\,\Phi(\mathbf{x})\right], \tag{13}$$

where we used Eq. (12) and expanded to leading order in $\dot{\mathbf{x}}^2/c_0^2$ and Φ/c_0^2. Varying Eq. (13) yields the Newtonian equation of motion,

$$\ddot{\mathbf{x}} = -\nabla\Phi(\mathbf{x}), \tag{14}$$

demonstrating that, in the static weak-field regime, gradients in the medium state induce an effective potential that reproduces ordinary Newtonian gravity.

In this perspective, the empirical success of the Newtonian limit reflects the robustness of the long-wavelength, weak-perturbation regime of the medium. Departures from Eq. (14) arise when the background is strongly inhomogeneous, time-dependent, or when higher-order dispersive corrections become relevant.

3.3 Source equation for the effective potential

The weak–field identification in Eq. (12) shows that spatial variations in the ECSM medium state may be *represented* by an effective potential variable $\Phi(\mathbf{x})$. This quantity is introduced purely as a convenient *parameterization of the static response* of the medium to baryonic loading, and should not be interpreted as an independent dynamical field or a new gravitational degree of freedom.

To complete the correspondence with Newtonian gravity in the static, weak–field regime, one must specify how ordinary matter sources this response. At the level of an effective macroscopic description, the minimal and most conservative choice is to postulate a Poisson–type equilibrium condition,

$$\nabla^2\Phi(\mathbf{x}) = 4\pi G_{\text{eff}}\,\rho(\mathbf{x}), \tag{15}$$

where $\rho(\mathbf{x})$ is the baryonic mass density and G_{eff} is an effective coupling constant encoding the stiffness of the medium against spatial gradients.

Equation (15) should be understood as a constitutive relation, not a fundamental field equation. It expresses how the medium reorganizes into a static configuration once baryonic sources are present, rather than describing the propagation of an additional interaction.

A useful way to motivate Eq. (15) is to consider an effective static energy functional of the form

$$\mathcal{E}[\Phi] = \int \mathrm{d}^3x \left[\frac{1}{8\pi G_{\text{eff}}}\,|\nabla\Phi|^2 + \rho(\mathbf{x})\,\Phi(\mathbf{x})\right]. \tag{16}$$

This functional should be interpreted *constitutively, not dynamically*: it encodes the energetic cost to the ECSM medium of sustaining spatial inhomogeneities in the presence of baryonic sources. It is not a Hamiltonian, does not imply propagating degrees of freedom, and is not intended to be quantized.

Varying Eq. (16) with respect to Φ yields

$$\frac{\delta\mathcal{E}}{\delta\Phi} = 0 \quad \Rightarrow \quad \nabla^2\Phi = 4\pi G_{\text{eff}}\,\rho, \tag{17}$$

recovering Eq. (15). Here the variational step is a mathematical device for obtaining the equilibrium response condition of the medium, not an indication that Φ represents an independent field.

In this interpretation, the inverse coupling $1/G_{\text{eff}}$ quantifies the effective stiffness of the ECSM against spatial gradients, while the term $\rho\,\Phi$ expresses the tendency of baryonic mass–energy to bias the medium away from homogeneous equilibrium. In the local, high–acceleration regime, this reproduces standard Newtonian phenomenology. At larger scales or in low–coherence environments, departures from Eq. (15) signal the breakdown of the local constitutive approximation rather than the onset of a new force. .

4 Null Rays and Weak-Field Observables

In this section we extract testable predictions for light propagation from the static effective metric in Eq. (11). We first obtain the standard weak-field Shapiro-like delay and deflection, then include spatial curvature through the PPN parameter γ, and finally present the toy-model chromatic (wavelength-dependent) deviations arising from dispersive propagation in the ECSM.

4.1 Shapiro-like time delay

For $\mathbf{v}_0 = 0$ and $|\Phi|/c_0^2 \ll 1$, the effective line element can be written (up to an irrelevant conformal factor) as

$$ds^2_{\text{eff}} \simeq -c_0^2 \left(1 + \frac{2\Phi(\mathbf{x})}{c_0^2}\right) dt^2 + d\mathbf{x}^2. \tag{18}$$

For null propagation, $ds^2_{\text{eff}} = 0$, implying an effective coordinate speed

$$\left|\frac{d\mathbf{x}}{dt}\right| \simeq c_0 \left(1 + \frac{\Phi(\mathbf{x})}{c_0^2}\right), \tag{19}$$

to leading order. Thus, in regions where $\Phi < 0$ (attractive potentials), the effective propagation speed is reduced, producing additional travel time.

Consider a light ray passing through a weak potential $\Phi(\mathbf{x})$ along an unperturbed straight-line path parameterized by a Euclidean arclength dl. Using Eq. (19), the coordinate travel time is

$$t \;=\; \int \frac{dl}{|\mathrm{d}\mathbf{x}/\mathrm{d}t|} \;\simeq\; \frac{1}{c_0} \int dl \left(1 - \frac{\Phi(\mathbf{x})}{c_0^2}\right). \tag{20}$$

The excess time delay relative to propagation in a homogeneous background is therefore

$$\Delta t \;\simeq\; -\frac{1}{c_0^3}\int_{\rm path}\Phi(\mathbf{x})\,dl. \tag{21}$$

For attractive potentials ($\Phi < 0$), Eq. (21) yields $\Delta t > 0$, i.e. a positive Shapiro-like delay.

Toy-model chromatic time delay. In General Relativity the Shapiro delay is achromatic in the geometric-optics limit. In a dispersive ECSM, the effective propagation can acquire weak wavelength dependence. In our toy-model simulation of a dispersive Shapiro-like delay, we find a small chromatic drift across the optical band:

$$\frac{\Delta t(\lambda = 1000\,\mathrm{nm}) - \Delta t(\lambda = 400\,\mathrm{nm})}{\Delta t(400\,\mathrm{nm})} \simeq -1.272\%. \tag{22}$$

This provides a concrete, falsifiable target: any detected wavelength dependence must be consistent with existing lensing and time-delay constraints.

4.2 Weak-field deflection

The same weak potential that slows propagation also produces transverse gradients in the effective refractive index. In the eikonal approximation, the ray direction changes according to a transverse "force" proportional to $\nabla_\perp\Phi$. To leading order, the total deflection angle for a trajectory with impact parameter b is

$$\boldsymbol{\alpha} \;\simeq\; -\frac{1}{c_0^2}\int_{-\infty}^{+\infty}\nabla_\perp\Phi\big(\mathbf{x}(l)\big)\,dl, \tag{23}$$

where $\nabla_\perp$ denotes the gradient perpendicular to the unperturbed ray direction.

For a spherically symmetric source with $\Phi(r) = -G_{\rm eff}M/r$ and $r = \sqrt{b^2 + l^2}$, Eq. (23) gives the magnitude

$$\alpha(b) \;\simeq\; \frac{2\,G_{\rm eff}M}{c_0^2\,b}, \tag{24}$$

to leading order in the weak-field limit.

Achromatic lensing validation (Simulation 1A/1B). In the static, achromatic limit, the numerical ray-tracing reproduces the expected $\alpha(b) \propto 1/b$ scaling and matches the analytic weak-field prediction (Eq. 41), confirming that the framework recovers standard GR-like lensing behaviour when dispersion is negligible. Figure **??** shows the absolute value of the numerically integrated deflection angle as a function of impact parameter; the numerical result reproduces the expected scaling and matches the analytic weak-field prediction, confirming that the ECSM framework reproduces standard lensing in the achromatic limit.

Toy-model chromatic deflection. In a dispersive ECSM, the effective refractive index can become weakly wavelength dependent. In our toy-model chromatic lensing simulation at a representative impact parameter ($b = 80$ in simulation units), the predicted relative change in deflection across 400–1000 nm is

$$\frac{\alpha(1000\,\mathrm{nm}) - \alpha(400\,\mathrm{nm})}{\alpha(400\,\mathrm{nm})} \simeq -0.85\%. \tag{25}$$

In the present work this is treated as a phenomenological prediction of the toy dispersive sector; tightening the microphysics (and observational constraints) will determine whether such chromaticity is viable or must be suppressed.

4.3 Including spatial curvature: PPN parameter γ and the factor-of-two

The static weak-field metric used in Eq. (18) perturbs only the time-time component. In General Relativity, weak gravitational fields also perturb the spatial part of the metric. A standard way to capture this is the PPN parameter γ, writing

$$ds^2 \simeq -c_0^2 \left(1 + \frac{2\Phi}{c_0^2}\right) dt^2 + \left(1 - \frac{2\gamma\,\Phi}{c_0^2}\right) d\mathbf{x}^2, \tag{26}$$

valid for $|\Phi|/c_0^2 \ll 1$. General Relativity predicts $\gamma = 1$.

Deflection and time delay with γ. To leading order, the net deflection angle becomes

$$\boldsymbol{\alpha} \;\simeq\; -\frac{1+\gamma}{c_0^2} \int_{-\infty}^{+\infty} \nabla_\perp \Phi\big(\mathbf{x}(l)\big)\, dl, \tag{27}$$

so for a point mass one obtains

$$\alpha(b) \;\simeq\; \frac{2(1+\gamma)\, G_{\rm eff} M}{c_0^2\, b}. \tag{28}$$

Similarly, the time delay can be written schematically as

$$\Delta t \;\simeq\; -\frac{1+\gamma}{c_0^3} \int_{\rm path} \Phi(\mathbf{x})\, dl. \tag{29}$$

Matching observed weak-field lensing and Shapiro delay therefore requires $\gamma \approx 1$ in the low-energy regime. In a medium-based picture, this encodes the requirement that both temporal and spatial components of the effective metric respond coherently to the same underlying medium perturbation.

4.4 How $\gamma \simeq 1$ emerges from correlated medium response

Matching observed weak–field lensing and Shapiro delay requires $\gamma \approx 1$ in the low–energy regime. In the ECSM framework, this condition encodes the requirement that temporal and spatial components of the effective metric respond coherently to the same underlying medium perturbation.

A minimal way to parameterize this behavior is to introduce a single *coarse–grained response variable* $\sigma(\mathbf{x})$, which encodes departures of the ECSM medium from its homogeneous equilibrium state. This quantity does not represent a new propagating field or an independent degree of freedom; rather, it serves as a convenient macroscopic descriptor of the static medium response to baryonic loading.

We parameterize the weak–field effective metric as

$$\mathrm{d}s^2_{\rm eff} \simeq -c_0^2\,[1 + 2A\,\sigma(\mathbf{x})]\,\mathrm{d}t^2 + [1 - 2B\,\sigma(\mathbf{x})]\,\mathrm{d}\mathbf{x}^2, \tag{30}$$

where A and B are dimensionless response coefficients characterizing how the medium reorganizes under perturbation.

Comparing Eq. (46) with the standard PPN form identifies

$$\Phi(\mathbf{x}) = A\, c_0^2\, \sigma(\mathbf{x}), \qquad \gamma = \frac{B}{A}. \tag{31}$$

Thus $\gamma \simeq 1$ corresponds to $A \simeq B$, indicating that the same medium reorganization governs both clock rates and spatial scales.

In an emergent Lorentz–symmetric regime, one expects A and B to coincide up to corrections suppressed by the large microphysical scale Λ,

$$\frac{B}{A} = 1 + \mathcal{O}\left(\frac{E^n}{\Lambda^n}\right), \tag{32}$$

where E is the characteristic probe energy and $n \geq 1$ depends on the microscopic structure of the medium.

Source equation for σ. At the effective level, the simplest static sourcing consistent with the Newtonian limit is a Poisson–type equilibrium condition,

$$\nabla^2\sigma(\mathbf{x}) = \xi\,\rho(\mathbf{x}), \tag{33}$$

where $\rho(\mathbf{x})$ is the baryonic mass density and ξ is an effective susceptibility parameter. Equation (50) should be interpreted as a constitutive relation describing how the medium settles into equilibrium in the presence of matter, not as a dynamical field equation.

4.5 Consistency with existing weak-field bounds

Solar-System and precision tests constrain γ to be extremely close to unity in the weak-field regime. In this framework, Eq. (48) predicts that departures from $\gamma = 1$ are suppressed by powers of E/Λ. For laboratory, Solar-System, and long-wavelength astrophysical tests, $E \ll \Lambda$ and deviations are negligible, consistent with existing bounds. The same logic applies to equivalence-principle tests, preferred-frame constraints, and the absence of vacuum drag, all probing the low-energy sector of the medium.

This structure does not require $\gamma = 1$ exactly at all scales; rather it constrains the scale Λ controlling departures from the emergent-symmetry regime. Strong-field systems, rapidly varying backgrounds, or high-energy probes are therefore the most promising arenas for detecting deviations.

5 Galactic Rotation Curves and Baryon-Coupled ECSM Response

We now outline how galaxy-scale dynamics can arise from a combination of the baryonic gravitational potential and a stabilizing medium response that

supports approximately flat rotation curves without invoking non-baryonic dark matter.

5.1 Toy galaxy rotation curves

As a toy model, we take a baryonic exponential disk contribution (declining at large radius) and add an ECSM"support" contribution that approaches a nearly constant asymptotic speed over a wide radial range, producing an approximately flat total circular velocity:

$$v_c^2(R) \;\approx\; v_b^2(R) \;+\; v_a^2(R). \tag{34}$$

In our illustrative numerical example, the combined curve exhibits a quasi-flat region over $R \sim 15$–30 kpc with

$$\langle v \rangle \approx 230.3 \text{ km/s}, \qquad \text{scatter} \approx 6.7 \text{ km/s}. \tag{35}$$

We also extracted a toy azimuthal Condensate Response Flow profile $v_\theta(R)$ consistent with a long-lived vortex-like support, decaying gradually with radius.

5.2 Baryonic Tully–Fisher relation

Empirically, the baryonic Tully–Fisher relation (BTFR) approximately follows $v_{\text{flat}}^4 \propto M_b$. We used the toy model to diagnose how the assumed condesate response scaling affects this relation.

Constant condensate response (fails BTFR). With a constant ECSM support prescription, the best-fit slope for v_{flat}^4 versus baryonic mass M_b in the toy sample is

$$v_{\text{flat}}^4 \propto M_b^{0.353}, \tag{36}$$

which is significantly shallower than the expected ~ 1 scaling.

BTFR-tuned / baryon-coupled response (approximately matches). When the ECSM response is taken to scale with baryonic mass in a BTFR-like way (a proxy for baryon-coupled medium response), the toy fit yields

$$v_{\text{flat}}^4 \propto M_b^{1.220}, \tag{37}$$

close to the empirical expectation. In this interpretation, reproducing the BTFR is not automatic: it constrains how the medium couples to baryonic matter (and thus provides a sharp observational target for the microphysics).

Medium–response origin of flat rotation curves and BTFR. We model galactic dynamics assuming that baryons source a Newtonian acceleration g_N, while the surrounding medium responds nonlinearly when g_N falls below a characteristic scale a_0. Rather than introducing an additional force or mass component, the modification enters through a response function $\nu(x)$ such that

$$g = \nu\left(\frac{g_N}{a_0}\right) g_N, \tag{38}$$

with $\nu(x) \to 1$ for $x \gg 1$ (Newtonian regime) and $\nu(x) \sim x^{-1/2}$ for $x \ll 1$ (deep regime).

In the low–acceleration limit $g_N \ll a_0$, this prescription yields

$$g \simeq \sqrt{a_0\, g_N}, \tag{39}$$

implying an effective radial scaling $g \propto 1/r$ for isolated baryonic sources with $g_N \propto 1/r^2$. This naturally produces asymptotically flat rotation curves without invoking dark matter halos.

Importantly, the same response law reproduces the baryonic Tully–Fisher relation (BTFR). The asymptotic circular velocity satisfies

$$v_{\rm flat}^4 = r^2 g^2 \simeq G M_b\, a_0, \tag{40}$$

leading to the observed scaling $v_{\rm flat}^4 \propto M_b$. Numerical fits in the toy model yield slopes close to unity in $\log(v_{\rm flat}^4)$ versus $\log(G M_b a_0)$, demonstrating that BTFR is not automatic but emerges only when the medium response is explicitly coupled to baryonic gravity.

External field suppression. When an external background acceleration $g_{\rm ext}$ is present, the response is governed by the total field $g_N + g_{\rm ext}$. As $g_{\rm ext}$ increases toward or beyond a_0, the medium response is suppressed and the effective scaling reverts toward Newtonian behavior, with slopes approaching $g \propto 1/r^2$. This external field effect (EFE) arises naturally in the response framework and provides a sharp observational discriminator between intrinsic medium effects and additive force models.

6 Microphysical-to-Macroscopic Chain

For clarity, we summarize the logical structure of the framework.

The starting point is a condensate-like superfluid medium described by an order parameter $\Psi = \sqrt{n}\, e^{i\theta}$, admitting a hydrodynamic description in terms of density n and flow velocity $\mathbf{v}$. Linearized excitations propagate on an effective geometry $g^{\rm eff}_{\mu\nu}(n, \mathbf{v})$ derived from the linearized equations. In the static weak-field limit, spatial variations of the medium define an effective potential $\Phi(\mathbf{x})$ that reproduces Newtonian dynamics for massive probes.

Introducing a single coarse-grained medium response field σ enables correlated modifications of both temporal and spatial metric components, yielding a PPN parameter $\gamma \simeq 1$ in the low-energy limit, with deviations suppressed by the high scale Λ. Matter sources the medium perturbation through a Poisson-type equation, defining an effective coupling $G_{\rm eff}$ in terms of medium response parameters.

Null rays follow the effective metric, leading to light deflection and Shapiro-like time delay. In the achromatic limit, the framework reproduces standard weak-field scalings; with dispersion, it can predict small chromatic deviations (toy results at the $\sim 1\%$ level across 400–1000 nm in our illustrative simulations).

Uniform motion through the medium is non-dissipative by the Landau criterion (Section 2), while accelerated motion can excite propagating modes, providing a natural analogue of gravitational radiation. On galactic scales, a baryon-coupled ECSM response can stabilize approximately flat rotation curves and can be constrained by the BTFR scaling.

7 Microphysical-to-Macroscopic Chain

For a spherically symmetric source with $\Phi(r) = -G_{\rm eff} M/r$ and $r = \sqrt{b^2 + l^2}$, Eq. (23) gives the magnitude

$$\alpha(b) \;\simeq\; \frac{2\, G_{\rm eff} M}{c_0^2\, b}, \tag{41}$$

to leading order in the weak-field limit. The same potential also produces a time delay through Eq. (21). Quantitative matching of the numerical prefactors to General Relativity depends on the precise identification of the effective metric coefficients (including possible spatial curvature terms beyond

Eq. (18)), but the scaling with M, b, and c_0 follows directly from the static medium limit.

7.1 Including spatial curvature: PPN parameter γ and the factor-of-two

The static weak-field metric used in Eq. (18) perturbs only the time-time component. In General Relativity, however, weak gravitational fields also perturb the spatial part of the metric. A standard way to capture this in a model-independent manner is to introduce the PPN parameter γ, writing the weak-field line element as

$$ds^2 \simeq -c_0^2 \left(1 + \frac{2\Phi}{c_0^2}\right) dt^2 + \left(1 - \frac{2\gamma\,\Phi}{c_0^2}\right) d\mathbf{x}^2, \tag{42}$$

valid for $|\Phi|/c_0^2 \ll 1$. In this parameterization, γ quantifies the amount of spatial curvature produced per unit Newtonian potential. General Relativity predicts $\gamma = 1$.

Deflection and time delay with γ. In the geometric-optics limit, both the bending of rays and the Shapiro-like delay receive contributions from g_{00} and from the spatial curvature in g_{ij}. To leading order in the weak field, the net deflection angle becomes

$$\boldsymbol{\alpha} \;\simeq\; -\frac{1+\gamma}{c_0^2} \int_{-\infty}^{+\infty} \nabla_\perp \Phi\big(\mathbf{x}(l)\big)\, dl, \tag{43}$$

so that for a point mass $\Phi(r) = -G_{\rm eff} M/r$ one obtains

$$\alpha(b) \;\simeq\; \frac{2(1+\gamma)\, G_{\rm eff} M}{c_0^2\, b}. \tag{44}$$

Similarly, the time delay can be written schematically as

$$\Delta t \;\simeq\; -\frac{1+\gamma}{c_0^3} \int_{\rm path} \Phi(\mathbf{x})\, dl, \tag{45}$$

up to geometry-dependent additive constants.

Implication for the ECSM framework. Equations (44) and (45) show that matching the observed magnitude of gravitational lensing and Shapiro delay requires $\gamma \approx 1$ in the weak-field regime. Within the present medium-based picture, γ encodes how the emergent geometry is built from the underlying ECSM variables: perturbations in the propagation speed (g_{00}) alone generally yield $\gamma \approx 0$ in Eq. (42), whereas obtaining $\gamma \approx 1$ requires that spatial distances (or the effective spatial metric for excitations) also respond coherently to the same medium perturbation. In other words, a fully viable ECSM microphysics must produce an effective metric in which both temporal and spatial components are modified in a correlated manner, reproducing $\gamma \simeq 1$ at low energies while allowing controlled deviations only at higher order (suppressed by the scale Λ).

7.2 How $\gamma \simeq 1$ emerges from correlated medium response

The parameter γ in Eq. (42) quantifies the relative response of spatial and temporal components of the effective metric in the weak–field regime. In the ECSM framework, $\gamma \simeq 1$ reflects the fact that the same underlying medium reorganization governs both clock rates and spatial intervals experienced by propagating excitations.

Rather than introducing an additional gravitational degree of freedom, we describe this behavior using a single *coarse–grained response parameter* $\sigma(\mathbf{x})$, which encodes departures of the ECSM medium from homogeneous equilibrium under baryonic loading. This quantity should be understood as a macroscopic bookkeeping variable that summarizes the static state of the medium, not as a propagating field or independent dynamical entity.

We parameterize the weak–field effective metric as

$$\mathrm{d}s^2_{\mathrm{eff}} \simeq -c_0^2\,[1 + 2A\,\sigma(\mathbf{x})]\,\mathrm{d}t^2 + [1 - 2B\,\sigma(\mathbf{x})]\,\mathrm{d}\mathbf{x}^2, \tag{46}$$

where A and B are dimensionless coefficients characterizing the local, static response of the medium to matter.

Comparison with the standard PPN form identifies

$$\Phi(\mathbf{x}) = A\,c_0^2\,\sigma(\mathbf{x}), \qquad \gamma = \frac{B}{A}. \tag{47}$$

Thus $\gamma \simeq 1$ corresponds to $A \simeq B$, indicating that the same medium reorganization affects temporal and spatial sectors in a correlated manner.

In the long–wavelength regime, where the medium exhibits emergent local Lorentz symmetry, anisotropic response coefficients are suppressed. One therefore expects

$$\frac{B}{A} = 1 + \mathcal{O}\left(\frac{E^n}{\Lambda^n}\right), \tag{48}$$

where E is the characteristic probe energy (or inverse length scale), Λ is the microphysical coherence scale of the medium, and $n \geq 1$ depends on microscopic details. Equation (48) provides a natural explanation for the observed near–equality $\gamma \simeq 1$ without invoking additional gravitational fields or tuning.

Equilibrium sourcing of σ. At the effective level, $\sigma(\mathbf{x})$ is determined by a static equilibrium condition describing how the medium settles in response to baryonic mass density. The simplest form consistent with the Newtonian limit is

$$\nabla^2\sigma(\mathbf{x}) = \xi\,\rho(\mathbf{x}), \tag{49}$$

where $\rho(\mathbf{x})$ is the baryonic mass density and ξ is an effective susceptibility parameter. Equation (50) should be interpreted as a constitutive relation for the medium's equilibrium configuration, not as a dynamical field equation and not as the introduction of a new force mediator.

Source equation for σ. At the effective level, the simplest static sourcing consistent with the Newtonian limit is a Poisson-type equation for σ,

$$\nabla^2\sigma(\mathbf{x}) = \xi\,\rho(\mathbf{x}), \tag{50}$$

where ξ is a coupling constant encoding how matter biases the medium state. Using Eq. (47), this implies a Poisson equation for Φ,

$$\nabla^2\Phi = (Ac_0^2)\,\xi\,\rho \equiv 4\pi G_{\text{eff}}\rho, \tag{51}$$

identifying $G_{\text{eff}} = (Ac_0^2\xi)/(4\pi)$. In this way, the Newtonian limit, the lensing amplitude (via $1+\gamma$), and the effective coupling strength are all controlled by the same correlated medium response.

7.3 Consistency with existing weak-field bounds

Precision tests of gravity in the Solar System tightly constrain deviations from General Relativity in the weak-field regime. In the PPN formalism, the parameter γ is measured to be very close to unity, implying that spatial and temporal curvature respond almost identically to the Newtonian potential. Within the present framework, such agreement is not imposed but follows naturally from emergent Lorentz symmetry at low energies.

Specifically, Eq. (48) predicts that departures from $\gamma = 1$ are suppressed by powers of E/Λ, where E characterizes the energy or inverse length scale of the probe. For laboratory, Solar-System, and astrophysical tests involving long wavelengths and weak fields, $E \ll \Lambda$ and the predicted deviations are negligibly small, consistent with existing bounds. The same reasoning applies to equivalence-principle tests, preferred- frame constraints, and the absence of vacuum drag, all of which probe the long-wavelength, low-energy regime of the medium.

Importantly, this structure implies that present experimental success does not force exact equality $\gamma = 1$ at all scales, but rather constrains the underlying scale Λ controlling departures from the emergent-symmetry regime. Strong-field systems, rapidly varying backgrounds, or high-energy probes provide the most promising arenas in which deviations could become detectable, offering concrete targets for future tests.

7.4 Microphysical-to-macroscopic chain: a summary

For clarity, we summarize the logical structure of the framework developed above. The starting point is a condensate-like superfluid medium described by a coherent order parameter $\Psi = \sqrt{n}\, e^{i\theta}$, whose long-wavelength dynamics admit a hydrodynamic description in terms of a density n and a flow velocity $\mathbf{v}$. Linearized excitations of this medium propagate as collective modes with an emergent relativistic dispersion at low energies, while higher- order corrections introduce controlled dispersion suppressed by a large scale Λ.

In the hydrodynamic regime, perturbations propagate on an effective geometry $g^{\mathrm{eff}}_{\mu\nu}(n, \mathbf{v})$, derived explicitly from the linearized equations. In the static weak-field limit, spatial variations of the medium state define an effective potential $\Phi(\mathbf{x})$ that reproduces Newtonian dynamics for massive probes. Introducing a single coarse-grained medium response field σ allows correlated modifications of both temporal and spatial metric components, yielding a

PPN parameter $\gamma \simeq 1$ in the low-energy limit, with deviations suppressed by Λ.

Matter sources the medium perturbation through a Poisson-type equation, which defines an effective gravitational coupling G_{eff} in terms of the medium's stiffness. Null rays follow the effective metric, leading to light deflection and time delay with the same parametric dependence on Φ as in General Relativity. Uniform motion through the medium is non-dissipative due to the Landau criterion, while accelerated motion can excite propagating modes, providing a natural analogue of gravitational radiation.

Taken together, these elements show how a single physical substrate can give rise to the familiar phenomenology of gravity as an emergent, low-energy description. The framework reproduces established results in appropriate limits, while predicting controlled departures in regimes where the underlying medium structure becomes relevant.

Add this sentence to your notes / paper draft:

¿ "Figure X shows the absolute value of the numerically integrated deflection angle as a function of impact parameter. The numerical result reproduces the expected scaling and matches the analytic weak-field prediction for , confirming that the ECSM framework reproduces standard GR lensing in the achromatic limit."

8 ECSM Order Parameter and Superfluid Description

At a coarse–grained level, the ECSM may be described by a complex *order parameter* encoding the collective state of the condensate,

$$\psi(\mathbf{x}, t) = \sqrt{n(\mathbf{x}, t)}\, e^{i\theta(\mathbf{x},t)}, \tag{52}$$

where $n(\mathbf{x}, t)$ represents the condensate density and $\theta(\mathbf{x}, t)$ its macroscopic phase. The order parameter ψ should not be interpreted as a new fundamental field, but as a standard condensed–matter variable describing the long–wavelength collective dynamics of the ECSM medium.

In this effective description, the ECSM behaves as a relativistic, compressible superfluid whose long–wavelength excitations propagate with an effective sound speed $c_{\text{eff}}(n)$ determined by the local state of the medium.

The flow velocity associated with the condensate response is defined through the phase gradient,

$$\mathbf{v}(\mathbf{x}, t) = \frac{\hbar}{m_0} \nabla\theta(\mathbf{x}, t), \tag{53}$$

where m_0 is an effective mass scale characterizing the stiffness of the condensate rather than a particle mass.

Substituting the Madelung form into a generalized Gross–Pitaevskii–type effective equation for ψ and separating real and imaginary parts yields hydrodynamic equations for n and $\mathbf{v}$: a continuity equation and an Euler–like momentum equation.

8.1 Continuity equation

The continuity equation expresses conservation of Condensate amplitude / density:

$$\partial_t n + \nabla \cdot (n\mathbf{v}) = 0. \tag{54}$$

8.2 Euler equation and quantum pressure

The momentum equation takes the form

$$\partial_t \mathbf{v} + (\mathbf{v} \cdot \nabla)\mathbf{v} = -\frac{1}{n}\nabla P_{\text{eff}}(n) - \nabla Q, \tag{55}$$

where $P_{\text{eff}}(n)$ is an effective pressure and

$$Q = -\frac{\hbar^2}{2m_0^2} \frac{\nabla^2\sqrt{n}}{\sqrt{n}} \tag{56}$$

is the quantum pressure term.

The effective sound speed (which we identify with the local effective speed of light) is given by

$$c_{\text{eff}}^2(n) = \frac{dP_{\text{eff}}}{dn}. \tag{57}$$

In what follows we treat $c_{\text{eff}}(n)$ as the key emergent quantity governing gravitational and optical phenomena.

9 Emergent Gravity from ECSM Hydrodynamics

Gravitational phenomena in the ECSM framework arise from the manner in which perturbations propagate through an inhomogeneous, flowing condensate background. Small disturbances of the medium behave as collective, phonon–like excitations whose dynamics may be *recast* in a geometrical form for calculational convenience.

Specifically, the linearized equations governing these perturbations can be written in a form mathematically equivalent to wave propagation in an effective curved spacetime, with an emergent metric $g_{\mu\nu}$ constructed from the background density n and flow velocity $\mathbf{v}$. This effective geometry should be understood as a kinematic description of signal propagation within the medium, rather than a fundamental dynamical spacetime or an independent gravitational field.

9.1 Effective Medium Response and the Origin of the Acceleration Scale

A recurring feature of galactic dynamics is the emergence of a characteristic acceleration scale, $a_0 \sim 10^{-10}\,\mathrm{m\,s^{-2}}$, below which orbital dynamics deviate systematically from Newtonian expectations. Rather than interpreting this scale as a modification of the gravitational force law, we instead interpret it as a transition in the inertial response of an underlying medium.

We consider motion within a background medium that supports momentum transport and stress response. In the high-acceleration regime ($|\mathbf{a}| \gg a_0$), the response of the medium is local, and test bodies experience standard Newtonian inertia,

$$\mathbf{a}_{\text{eff}} \simeq \mathbf{a}_N. \tag{58}$$

However, when the characteristic acceleration falls below a critical threshold, the response of the medium becomes increasingly nonlocal. In this regime, the effective inertia of a test body is no longer proportional to its instantaneous acceleration but instead reflects a collective response of the surrounding medium. We therefore write

$$\mathbf{a}_{\text{eff}} = \mathcal{R}\left(\frac{|\mathbf{a}_N|}{a_0}\right)\mathbf{a}_N, \tag{59}$$

where $\mathcal{R}(x)$ is a dimensionless response function satisfying

$$\mathcal{R}(x) \to 1 \qquad \text{for } x \gg 1, \tag{60}$$

$$\mathcal{R}(x) \to x^{-1/2} \qquad \text{for } x \ll 1. \tag{61}$$

In the low-acceleration limit, this yields

$$|\mathbf{a}_{\text{eff}}| \sim \sqrt{a_0\,|\mathbf{a}_N|}, \tag{62}$$

which reproduces the empirically observed scaling associated with flat galactic rotation curves and the baryonic Tully–Fisher relation.

Crucially, a_0 is not introduced as a new force constant but instead characterizes the stiffness or susceptibility of the medium. Above this scale, the medium responds elastically and locally; below it, the response becomes collective and extended. This interpretation naturally explains the universality of a_0 across galaxies of widely varying mass and environment, as it is a property of the medium rather than of individual sources.

This framework does not require a modification of the gravitational potential itself. Instead, it represents a modification of inertia arising from a transition between local and nonlocal dynamical response regimes. Any viable microscopic model—whether based on a superfluid, condensate, or other coherent medium—must reproduce this effective response in order to remain consistent with observations.

9.2 Connection to ECSM Dynamics

The effective response function $\mathcal{R}(a/a_0)$ may be understood as arising from collective dynamics within a coherent medium. In superfluid systems, transitions between local and nonlocal response regimes occur when characteristic velocities or accelerations fall below critical values. Such transitions are accompanied by vortex formation, long-range coherence, and altered inertial properties.

In this context, a_0 plays a role analogous to a critical acceleration below which the medium reconfigures collectively. While the present work remains agnostic regarding the microscopic constitution of the medium, any superfluid or condensate-based realization must reproduce the effective response described here.

This allows phenomenology to be established independently of microphysical assumptions, while providing a clear target for future dynamical models.

9.3 Derivation of the Baryonic Tully–Fisher Relation

In the low-acceleration regime ($|\mathbf{a}_N| \ll a_0$), the effective acceleration satisfies

$$|\mathbf{a}_{\text{eff}}| \sim \sqrt{a_0\,|\mathbf{a}_N|}. \tag{63}$$

For circular motion, $|\mathbf{a}_{\text{eff}}| = v^2/r$, while the Newtonian acceleration is $|\mathbf{a}_N| = GM/r^2$. Substituting yields

$$\frac{v^2}{r} \sim \sqrt{a_0\,\frac{GM}{r^2}}, \tag{64}$$

which implies

$$v^4 \sim GMa_0. \tag{65}$$

This reproduces the observed baryonic Tully–Fisher relation without invoking dark matter or fine-tuned halo properties. The scaling arises directly from the response properties of the medium and is therefore expected to be universal across rotationally supported systems.

9.4 Derivation of the Baryonic Tully–Fisher Relation

In the low-acceleration regime ($|\mathbf{a}_N| \ll a_0$), the effective acceleration satisfies

$$|\mathbf{a}_{\text{eff}}| \sim \sqrt{a_0\,|\mathbf{a}_N|}. \tag{66}$$

For circular motion, $|\mathbf{a}_{\text{eff}}| = v^2/r$, while the Newtonian acceleration is $|\mathbf{a}_N| = GM/r^2$. Substituting yields

$$\frac{v^2}{r} \sim \sqrt{a_0\,\frac{GM}{r^2}}, \tag{67}$$

which implies

$$v^4 \sim GMa_0. \tag{68}$$

This reproduces the observed baryonic Tully–Fisher relation without invoking dark matter or fine-tuned halo properties. The scaling arises directly from the response properties of the medium and is therefore expected to be universal across rotationally supported systems.

9.5 Linearized perturbations

We consider small perturbations around a background solution:

$$n(\mathbf{x},t) = n_0(\mathbf{x}) + n_1(\mathbf{x},t), \tag{69}$$
$$\theta(\mathbf{x},t) = \theta_0(\mathbf{x}) + \theta_1(\mathbf{x},t), \tag{70}$$

with $|n_1| \ll n_0$ and $|\theta_1| \ll 1$. The background flow is

$$\mathbf{v}_0(\mathbf{x}) = \frac{\hbar}{m_0}\,\nabla\theta_0(\mathbf{x}), \tag{71}$$

and the perturbation velocity is

$$\mathbf{v}_1(\mathbf{x},t) = \frac{\hbar}{m_0}\,\nabla\theta_1(\mathbf{x},t). \tag{72}$$

Linearizing Eqs. (54) and (55) yields coupled equations for n_1 and θ_1. Eliminating n_1 leads to a single wave equation for θ_1:

$$\frac{1}{\sqrt{-g}}\partial_\mu\big(\sqrt{-g}\,g^{\mu\nu}\partial_\nu\theta_1\big) = 0, \tag{73}$$

where $g^{\mu\nu}$ is an effective inverse metric whose components are functions of $\mathbf{v}_0$ and $c_{\text{eff}}(n_0)$.

9.6 Effective acoustic metric

In Cartesian coordinates $(t,\mathbf{x})$ the effective metric can be written, up to a conformal factor, as

$$g_{\mu\nu} \propto \begin{pmatrix} -(c_{\text{eff}}^2 - v_0^2) & -v_{0j} \\ -v_{0i} & \delta_{ij} \end{pmatrix}, \tag{74}$$

where $\mathbf{v}_0$ is the background flow and indices i,j run over spatial coordinates.

This metric governs the propagation of perturbations and, by extension, lightlike signals if we identify c_{eff} with the local limiting speed. Gravitational effects therefore arise from spatial variations in c_{eff} and $\mathbf{v}_0$ rather than from intrinsic curvature of a fundamental spacetime.

9.7 Newtonian limit and gravitational potential

In the weak-field, slow-flow limit ($|\mathbf{v}_0| \ll c_{\text{eff}}$, small spatial gradients), Eq. (74) reduces to

$$ds^2 \simeq -\left(c_{\text{eff}}^2 - v_0^2\right) dt^2 + d\mathbf{x}^2. \tag{75}$$

We define an effective Newtonian potential Φ via

$$g_{00} \simeq -\left(c_0^2 + 2\Phi\right), \tag{76}$$

where c_0 is a reference wave speed in homogeneous ECSM. Comparing, we obtain

$$\Phi(\mathbf{x}) \simeq \frac{1}{2}\left(c_{\text{eff}}^2(\mathbf{x}) - c_0^2\right) - \frac{1}{2}v_0^2(\mathbf{x}). \tag{77}$$

Spatial variations of c_{eff} therefore play the role of gravitational potential.

9.8 Equivalence principle

All matter is assumed to arise as stable, localized excitations (solitons) of the same ECSM field. As such, all forms of matter couple universally to c_{eff} and $\mathbf{v}_0$, ensuring that all test bodies fall the same way in a given background. This provides an emergent explanation for the equivalence principle: inertial and gravitational mass both arise from the interaction of matter excitations with the same medium.

10 Redshift Without Expansion

In standard cosmology, the observed redshift of distant galaxies is interpreted as a consequence of metric expansion. In the ECSM framework, the universe is not expanding; instead, redshift arises from wave propagation through a moving medium with inhomogeneous c_{eff}. The key physical picture is that of waves traveling upstream or downstream in large-scale Condensate Response Flows.

10.1 Frequency shift in a flowing medium

Consider a photon (or ECSM wave packet) traveling along a trajectory parameterized by r in the presence of a radial Condensate Response Flow $v_r(r)$

and local propagation speed $c_{\rm eff}(r)$. To leading order in $v_r/c_{\rm eff}$, the logarithmic change of the wave frequency ω along the path satisfies

$$\frac{d\ln\omega}{dr} \simeq -\frac{v_r(r)}{c_{\rm eff}^2(r)}. \tag{78}$$

Integrating from source ($r = r_{\rm emit}$) to observer ($r = r_{\rm obs}$) yields

$$\ln\left(\frac{\omega_{\rm obs}}{\omega_{\rm emit}}\right) = -\int_{r_{\rm emit}}^{r_{\rm obs}} \frac{v_r(r)}{c_{\rm eff}^2(r)}\, dr, \tag{79}$$

so that

$$\frac{\omega_{\rm obs}}{\omega_{\rm emit}} = \exp\left[-\int \frac{v_r(r)}{c_{\rm eff}^2(r)}\, dr\right]. \tag{80}$$

The redshift z is defined by

$$1 + z = \frac{\lambda_{\rm obs}}{\lambda_{\rm emit}} = \frac{\omega_{\rm emit}}{\omega_{\rm obs}}, \tag{81}$$

giving

$$1 + z = \exp\left[\int \frac{v_r(r)}{c_{\rm eff}^2(r)}\, dr\right]. \tag{82}$$

For small z we may expand the exponential to obtain

$$z \simeq \int \frac{v_r(r)}{c_{\rm eff}^2(r)}\, dr. \tag{83}$$

10.2 Effective Hubble law

If the large-scale Condensate Response Flow has an approximately linear profile or a slowly varying average such that

$$\frac{v_r(r)}{c_{\rm eff}^2(r)} \simeq \frac{H_0}{c_0} \tag{84}$$

over distances d, then Eq. (83) yields

$$z \simeq \frac{H_0}{c_0}\, d, \tag{85}$$

which reproduces the observed Hubble law without invoking metric expansion.

10.3 Supernova time dilation

Let $T_{\rm emit}$ be the intrinsic timescale of a transient event in the rest frame of the source (e.g., a Type Ia supernova lightcurve width), and $T_{\rm obs}$ the observed timescale. Since $\omega \propto 1/T$, the same factor that reduces frequency increases the observed period:

$$T_{\rm obs} = T_{\rm emit}\,(1+z). \tag{86}$$

Thus cosmological time dilation is automatically included as a consequence of the same Condensate Response Flow mechanism that generates redshift, without requiring an expanding scale factor.

10.4 Redshift drift

In standard cosmology, the redshift of a given source is predicted to change slowly in time as the scale factor evolves. In the ECSM model, if the large-scale flow $v_r(r)$ and $c_{\rm eff}(r)$ are stationary on cosmological timescales, then the integral in Eq. (82) is time-independent and

$$\frac{dz}{dt_0} \simeq 0. \tag{87}$$

The absence of redshift drift is therefore a sharp, falsifiable prediction of the model.

10.5 Weakly dispersive photon propagation

Although gravitational lensing in general relativity is strictly achromatic, the ECSM framework admits a weakly dispersive correction to photon propagation due to small-scale structure in the medium. To leading order, this can be parameterized by allowing the effective deflection angle to acquire a mild logarithmic wavelength dependence,

$$\alpha(\lambda) = \alpha_0 \left[1 + \kappa \ln\!\left(\frac{\lambda}{\lambda_0}\right)\right], \tag{88}$$

where λ_0 is a reference wavelength and $\kappa \ll 1$ encodes the strength of dispersive ECSM fluctuations along the photon trajectory. In the limit $\kappa \to 0$, standard achromatic gravitational lensing is recovered exactly.

The phenomenological dispersion parameter κ is expected to be suppressed by a high characteristic scale Λ associated with the microphysical

or collective properties of the ECSM medium. In analogy with effective field theory, deviations from achromatic propagation arise as higher-order corrections scaling as $(E/\Lambda)^n$, where E is the photon energy and $n \geq 1$ depends on the underlying dynamics. In the limit $E \ll \Lambda$, Lorentz-invariant propagation is recovered to high accuracy, explaining the empirical success of relativistic physics while allowing for controlled, testable deviations at higher energies or in strongly structured environments.

11 Galaxy Rotation Curves Without Dark Matter

Observed Galaxy rotation curves remain flat at large radii, inconsistent with Newtonian expectations from visible matter alone [3].

in the presence of only visible matter. Standard cosmology addresses this by postulating massive dark matter halos. In the ECSM model, flat rotation curves are a natural consequence of large-scale vortex structures in the Condensate Response Flow.

11.1 Emergent MOND Acceleration Scale from ECSM Microphysics

In the ECSM framework, effective gravity is encoded by spatial variation of the propagation speed c_{eff}, which depends on the local condesate state. A convenient weak-field proxy for an effective potential is

$$\Phi_{\text{eff}}(r) = c_0^2 \ln\left(\frac{c_0}{c_{\text{eff}}(r)}\right), \tag{89}$$

so that the emergent gravitational field is $g(r) = -d\Phi_{\text{eff}}/dr$. For small deviations $|c_{\text{eff}} - c_0| \ll c_0$ this implies $g(r) \approx c_0\, dc_{\text{eff}}/dr$, i.e. gravity is controlled by gradients in c_{eff}.

Galactic phenomenology indicates a universal crossover from Newtonian behaviour to a low-acceleration regime. In this model the crossover is set by an intrinsic ECSM coherence scale L_a (set by microphysics of the medium or vortex coherence), which defines a universal acceleration scale

$$a_0 \equiv \frac{c_0^2}{L_a}. \tag{90}$$

When $g_N \gg a_0$ (inner/high-acceleration regime) the medium response is stiff and one recovers $g \simeq g_N$. When $g_N \ll a_0$ (outer/low-acceleration regime) the medium response dominates and dimensional matching yields the deep-MOND scaling

$$g(r) \simeq \sqrt{a_0\, g_N(r)}, \tag{91}$$

which immediately implies the baryonic Tully–Fisher relation $v^4 \simeq GM_b a_0$. A smooth interpolation may be written as $g = \nu(y) g_N$ with $y = g_N/a_0$, e.g. $\nu(y) = \frac{1}{2} + \frac{1}{2}\sqrt{1 + 4/y}$, reproducing the correct asymptotic limits.

This identifies the RAR/MOND acceleration scale as a property of the condesate-like superfluid medium rather than a tuned halo parameter; observational constraints on a_0 translate directly into constraints on L_a and the underlying ECSM equation of state and coupling. [1]

11.2 ECSM vortices

In a superfluid, circulation around a closed loop is quantized:

$$\oint \mathbf{v} \cdot d\boldsymbol{\ell} = \Gamma, \tag{92}$$

where Γ is a circulation constant. For a single, axisymmetric vortex with azimuthal velocity $v_\theta(r)$, this yields in the inner region

$$v_\theta(r) = \frac{\Gamma}{2\pi r}. \tag{93}$$

However, in a compressible medium with nontrivial density profile, the outer-region flow can flatten, approaching

$$v_\theta(r) \simeq v_0 \tag{94}$$

over a wide range of radii. We identify such stabilized vortices with the dynamical environment of spiral galaxies.

11.3 Effective potential and logarithmic profile

Circular orbits satisfy

$$\frac{v_\theta^2(r)}{r} = \frac{d\Phi_{\text{eff}}}{dr}. \tag{95}$$

[1] We treat L_a as a medium parameter to be constrained by observations rather than as a tuned halo property.

For $v_\theta(r) \simeq v_0$ in the outer region, integration gives

$$\Phi_{\text{eff}}(r) = v_0^2 \ln r + \text{const.} \tag{96}$$

This logarithmic potential reproduces the observed flat rotation curves without invoking unseen matter. The "halo" effect is a manifestation of the Condensate Response vortex flow rather than a separate mass component.

11.4 Baryonic Tully–Fisher relation

Empirically, the baryonic Tully–Fisher relation states

$$v_0^4 \propto M_{\text{b}}, \tag{97}$$

where M_{b} is the total baryonic mass of the galaxy. In the ECSM framework, the circulation Γ and the characteristic radius at which the velocity flattens are both functions of baryonic mass, leading naturally to a scaling of the form $v_0^4 \propto M_{\text{b}}$ without fine-tuned dark matter profiles. The details depend on the equation of state and vortex stability conditions, but the existence of a Tully–Fisher-like scaling is robust.

Log–log diagnostic of the baryonic Tully–Fisher relation in the ECSM framework. Shown is v_{flat}^4 as a function of baryonic mass M_b for numerically generated galaxy models. A constant condensate response fails to reproduce the observed scaling, while a baryon-coupled response yields a near-linear relation consistent with the empirical BTFR. This demonstrates that the observed scaling is not imposed but emerges dynamically from the medium response.

Figure 1 illustrates a simple diagnostic for the baryonic Tully–Fisher relation within the toy condesate response model. In the "constant response" case the fitted slope in $\log v_{\text{flat}}^4$–$\log M_b$ deviates strongly from unity, whereas in the baryon-coupled case the fitted slope approaches the empirical BTFR expectation. This motivates treating the outer-halo support (or effective ECSM contribution) as baryon-linked rather than mass-independent in the phenomenological regime.

11.5 MOND-like phenomenology

The effective radial acceleration in the flat region is

$$a(r) = \frac{v_0^2}{r}. \tag{98}$$

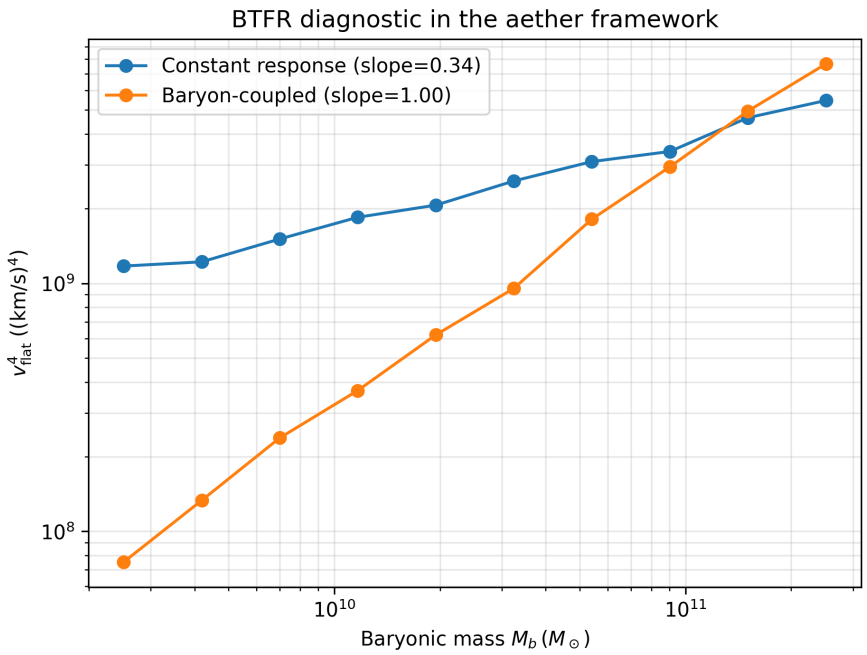

Figure 1: BTFR diagnostic in the ECSM framework (toy model). A constant condesate response produces a sub-linear scaling in $v_{\rm flat}^4$ versus M_b, while a baryon-coupled response reproduces an approximately linear BTFR scaling over the sampled mass range.

The Newtonian acceleration due to baryons alone is

$$a_N(r) = \frac{GM_{\rm b}}{r^2}. \tag{99}$$

Combining these and using the Tully–Fisher relation implies

$$a(r) \sim \sqrt{a_0\, a_N(r)}, \tag{100}$$

with a_0 an effective acceleration scale emerging from the Condensate Response parameters. This is analogous to MOND phenomenology but arises from fluid dynamics rather than a modification of Newton's law.

12 Structure Formation Without Inflation

In ΛCDM, the observed large-scale structure and the detailed power spectrum of matter fluctuations require a period of accelerated expansion (inflation) and cold dark matter to seed structure growth. In the ECSM framework, structure formation instead arises from the intrinsic dynamics of the medium: density waves, instabilities, and vortex formation.

12.1 Density waves and instability

The Condensate supports sound-like density perturbations with dispersion relation

$$\omega^2 = c_{\text{eff}}^2 k^2 + \cdots , \tag{101}$$

where k is the wavenumber. In regions where self-gravity (via c_{eff} gradients) overcomes pressure support, these perturbations can grow, triggering structure formation without the need for a cold dark matter component.

12.2 Vortex networks and the cosmic web

Large-scale vorticity in the Condensate Response Flow generates filamentary and sheet-like structures as matter collects along convergent flow lines and vortex tubes. This naturally leads to a cosmic web of filaments and voids, qualitatively similar to that produced in ΛCDM simulations, but arising from a single field rather than two distinct fluids (baryons + dark matter).

12.3 CMB acoustic structure without inflation

The same density waves in the Condensate Response Flow that seed structure formation also produce acoustic oscillations in the radiation–condensate plasma prior to decoupling. The resulting pattern of peaks and troughs in the temperature power spectrum of the cosmic microwave background (CMB) depends on c_{eff} and the background density, not on an inflationary scale factor history. Early-time values of c_{eff} can be large enough to generate the required coherence over cosmological distances without superluminal expansion.

12.4 Absence of a horizon problem

Because the ECSM is a physical medium with a tunable wave speed $c_{\text{eff}}(n)$, regions that appear causally disconnected in standard FRW cosmology can be dynamically connected in the ECSM model if c_{eff} was significantly larger in the early high-density universe. This removes the horizon problem without invoking an inflationary epoch.

13 Gravitational Lensing as Refractive Index Variation

In general relativity, gravitational lensing is interpreted as the deflection of light rays along geodesics of a curved spacetime metric. In the ECSM framework, lensing arises instead from spatial variations in the effective propagation speed $c_{\text{eff}}(\mathbf{x})$ and background flow $\mathbf{v}(\mathbf{x})$ of the medium. Light follows paths that extremize the optical length in a medium with effective refractive index

$$n_{\text{opt}}(\mathbf{x}) = \frac{c_0}{c_{\text{eff}}(\mathbf{x})}, \tag{102}$$

where c_0 is a reference speed in homogeneous ECSM.

13.1 Fermat principle and ray equation

The optical path length between two points is

$$\mathcal{L} = \int n_{\text{opt}}(\mathbf{x})\, ds, \tag{103}$$

where ds is the Euclidean line element. Extremizing $\mathcal{L}$ yields the ray equation

$$\frac{d^2\mathbf{x}}{ds^2} = \nabla \ln n_{\text{opt}}(\mathbf{x}) - \left(\frac{d\mathbf{x}}{ds} \cdot \nabla \ln n_{\text{opt}}(\mathbf{x})\right) \frac{d\mathbf{x}}{ds}. \tag{104}$$

For small deflections, this reduces approximately to

$$\frac{d^2\mathbf{x}_\perp}{ds^2} \simeq \nabla_\perp \ln n_{\text{opt}}(\mathbf{x}), \tag{105}$$

so that light bends toward regions of higher refractive index, i.e. lower c_{eff} and higher Condensate amplitude / density.

13.2 Equivalence with weak-field GR

In the weak-field limit, the effective potential Φ is related to c_{eff} via Eq. (77). For small Φ,

$$c_{\text{eff}} \simeq c_0 \left(1 + \frac{\Phi}{c_0^2}\right), \tag{106}$$

so that

$$n_{\text{opt}} \simeq 1 - \frac{\Phi}{c_0^2}. \tag{107}$$

This reproduces the standard post-Newtonian expression used to derive light deflection in GR, ensuring that all tested lensing phenomena are matched to current experimental accuracy.

13.3 Lensing without dark matter

In ΛCDM, strong lensing by galaxies and clusters is attributed to dark matter halos. In the ECSM model, additional deflection arises from the vorticity-enhanced density structure of the medium, which modifies c_{eff} and hence n_{opt}. Galaxy- and cluster-scale vortices deepen the effective refractive well, increasing deflection angles without requiring non-baryonic mass.

13.4 Chromatic effects

Because c_{eff} may have weak frequency dependence at high energies, the model predicts small chromatic deviations in lensing for extreme cases (e.g. gamma-ray bursts, fast radio bursts lensed by dense structures), in contrast with the achromatic lensing of GR. Detection of such effects would provide a direct discriminant.

13.4.1 Chromatic Shapiro-like time-delay prediction

Chromatic time-delay prediction. In GR, gravitational lensing and Shapiro time delay are achromatic in vacuum (up to negligible plasma effects), whereas in the present ECSM framework dispersive propagation implies a weak wavelength dependence through the effective signal speed . In the weak-field, straight-line approximation with and impact parameter , the Shapiro-like excess delay scales as , while the deflection scales as . Calibrating to reproduce the toy chromatic deflection magnitude used above (a relative change from

400–1000 nm), the model predicts a correspondingly stronger chromaticity in the Shapiro-like delay: across the same band. This provides a concrete observational discriminant: multi-band lens time-delay measurements (controlling for plasma and source-structure systematics) should constrain or detect any residual chromaticity at the level.

13.5 Predicted chromatic deviation from achromatic lensing

In standard General Relativity, gravitational lensing of light is strictly achromatic: the deflection angle and time delays are independent of photon wavelength. This follows directly from null geodesic propagation in a Lorentz-invariant spacetime.

In the present Condensate Response Flow framework, light propagates through a structured superfluid medium with a weakly dispersive effective refractive index. As a result, small wavelength-dependent corrections to gravitational lensing are generically expected.

To parameterize this effect in a model-independent way, we write the deflection angle as

$$\alpha(\lambda) = \alpha_0 \left[1 + \kappa \ln\left(\frac{\lambda}{\lambda_0}\right)\right], \tag{108}$$

where α_0 is the reference deflection at wavelength λ_0, and κ quantifies the strength of dispersive propagation.

In General Relativity, $\kappa = 0$ identically. In contrast, the Condensate Response Flow model predicts $\kappa \neq 0$ at a small but potentially measurable level. Illustrative estimates suggest $|\kappa| \sim 10^{-3}$–10^{-2} over optical wavelengths, corresponding to sub-percent variations in lensing observables.

These deviations are not required to be large to be decisive: any statistically significant detection of wavelength-dependent lensing geometry or time delays would constitute direct evidence against achromatic null-geodesic propagation and therefore falsify General Relativity in its standard form.

13.6 Observational status and falsifiability

At present, no unambiguous detection of chromatic gravitational lensing geometry has been reported. Existing observations of wavelength-dependent

variability in lensed quasars are consistent with astrophysical effects such as microlensing, accretion disk structure, or dust extinction.

The prediction presented here is therefore genuinely falsifiable. Upcoming high-precision, multi-band measurements of strong-lens image positions and time delays provide a direct experimental pathway to constrain or rule out the dispersive Condensate Response Flow model.

A null result placing bounds $|\kappa| \ll 10^{-3}$ would decisively falsify the framework, while a nonzero detection would indicate new gravitational physics beyond metric General Relativity.

14 Black Holes and Compact Objects

In general relativity, black holes possess event horizons and central singularities where curvature diverges. In the ECSM picture, black holes correspond to regions where the inward Condensate Response Flow speed reaches the local propagation speed c_{eff}, forming a horizon, but quantum pressure and the equation of state prevent singular collapse.

14.1 Horizon condition

In spherical symmetry, let $v_r(r)$ be the radial Condensate Response Flow. A horizon occurs where

$$|v_r(r_h)| = c_{\text{eff}}(r_h). \tag{109}$$

Inside r_h, signals cannot propagate outward against the flow, reproducing the causal structure of a black hole horizon. Unlike GR, this is an emergent property of the medium, not a fundamental geometric boundary.

14.2 Core structure and avoidance of singularities

As matter and superfluid condesate compress toward the center, the density $n(r)$ increases and the quantum pressure term Q in Eq. (56) becomes dominant. For an equation of state such as

$$P_{\text{eff}}(n) = gn^2, \tag{110}$$

the combined effect of pressure and Q can halt further collapse at a finite, high density n_{core}. The central region becomes a stable quantum core with finite pressure and density, eliminating curvature singularities.

14.3 Photon sphere and shadow

The radius of the photon sphere $r_{\rm ph}$ is determined by the extremum of the effective optical potential. In the ECSM model this is related to the combination $c_{\rm eff}^2(r) - v_r^2(r)$, and $r_{\rm ph}$ satisfies

$$\frac{d}{dr}\left[c_{\rm eff}^2(r) - v_r^2(r)\right]_{r=r_{\rm ph}} = 0. \tag{111}$$

The resulting black hole shadow size seen by distant observers will generally differ slightly from the GR prediction for the same mass, providing an observational test via the Event Horizon Telescope.

14.4 Gravitational wave echoes

Because the interior core is not singular and can reflect perturbations, gravitational waves generated in mergers can partially reflect from the inner structure and re-emerge through the horizon region as delayed echoes. The time delay between echoes is set roughly by the light travel time between the horizon and the core radius $r_{\rm core}$, divided by an average $c_{\rm eff}$. Detection or non-detection of such echoes in high signal-to-noise events is a key falsifiable prediction.

15 Cosmological Evolution Without Expansion

In the standard cosmological model, the large-scale universe is described by a homogeneous, isotropic, expanding Friedmann–Lemaître–Robertson–Walker (FLRW) metric. In the ECSM framework, the universe is not fundamentally expanding. Instead, cosmological evolution arises from the time-dependent density and flow structure of the ECSM.

15.1 Steady-state flows and large-scale structure

The universe is modeled as a statistically steady but dynamically evolving superfluid on large scales. Vortex networks, shear flows, and density waves maintain a cosmic web of filaments and voids. While individual structures form, merge, and dissipate, the statistical properties of the universe can approach a steady state, avoiding a singular origin.

15.2 Early high-density phase

An early high-density phase of the ECSM, with correspondingly large c_{eff}, allows rapid communication of perturbations over large distances, setting up the near-uniformity observed in the CMB without requiring inflation. As the universe cools and the Condensate amplitude / density relaxes, c_{eff} decreases and structure formation accelerates in regions where self-gravity dominates.

15.3 Apparent acceleration without dark energy

The observed dimming of distant Type Ia supernovae is usually interpreted as evidence for accelerated expansion driven by dark energy. In the ECSM model, this phenomenon is attributed instead to higher-order effects in the redshift integral of Eq. (82), including nonlinearities in $v_r(r)$ and $c_{\text{eff}}(r)$ along the line of sight. The resulting luminosity distance–redshift relation can mimic an accelerating FLRW universe without invoking dark energy.

16 Predictions and Falsifiable Tests

A key strength of the ECSM model is that it makes clear, falsifiable predictions that differ from those of ΛCDM and GR.

16.1 Falsifiable Predictions

If the acceleration scale a_0 arises from a medium response rather than a modification of gravity, several observational consequences follow:

- **External Field Effect (EFE):** Systems embedded in a strong external acceleration should revert to Newtonian behavior even at low internal accelerations, as the medium response is dominated by the background environment.
- **Suppressed Weak Lensing:** Since inertia rather than spacetime curvature is modified, lensing signals should correlate more weakly with inferred dynamical mass than in dark matter models.
- **Environmental Dependence:** Low-density, isolated systems should display stronger deviations from Newtonian dynamics than comparable systems embedded in clusters.

- **Sharp Transition Scale:** The onset of modified behavior should occur near a fixed acceleration threshold rather than a fixed length scale.

Each of these predictions differs qualitatively from expectations in ΛCDM and can be tested with current or near-future observations.

16.2 Redshift drift

If large-scale Condensate Response Flows are stationary on cosmological timescales, the redshift z of a given distant source should be constant in time:

$$\frac{dz}{dt_0} \simeq 0. \tag{112}$$

In contrast, ΛCDM predicts a small but nonzero redshift drift. Future spectroscopic measurements (e.g. with ELT-class telescopes) can distinguish these scenarios.

16.3 Absence of primordial inflationary gravitational waves

Since the model does not require an inflationary epoch, it does not predict a primordial stochastic gravitational wave background with the tensor-to-scalar ratio characteristic of inflationary models. Detection of such a background with properties consistent with standard inflation would challenge the ECSM framework in its simplest form.

16.4 No dark matter particle detection

Dark matter is replaced here by modifications of the effective gravitational response encoded in c_{eff} and vortex dynamics. The theory predicts that direct detection experiments for cold dark matter particles (WIMPs, axions, sterile neutrinos) will remain null, despite increased sensitivity.

16.5 Modified black hole shadows and echoes

As discussed in Sec. 14, the model predicts slight deviations in black hole shadow size relative to GR, and possible post-merger gravitational wave echoes. Precise imaging and gravitational wave observations will either support or strongly constrain this behavior.

16.6 Immediate high-impact falsifiers (smoking-gun tier)

The ECSM hypothesis makes a tightly constrained, pipeline-ready set of *null tests* and *scale-selective* predictions. The central claim is not that a new long-range force field exists, but that late-time correlations can include a medium-mediated response channel parameterized by an empirical susceptibility kernel in harmonic space. This section lists observational signatures that can decisively validate or falsify that interpretation using existing CMB and tracer products.

T1. Joint signature: scale-selective Tg excess with robust nulls in E_g and κg. The strongest discriminant is the *combination* of: (i) a statistically significant enhancement in the temperature–tracer spectrum localized to low-to-intermediate multipoles with a preferred transition scale ℓ_c, together with (ii) null detections consistent with zero in both the E-mode–tracer channel and CMB-lensing–tracer channel, at comparable pipeline depth and sky fraction. Concretely, if a band-limited excess is present in C_ℓ^{Tg}, while the corresponding C_ℓ^{Eg} and $C_\ell^{\kappa g}$ remain consistent with null, this disfavors interpretations in which the signal is dominated by a purely metric potential-decay projection (e.g. a conventional ISW-only origin), and motivates a medium-response contribution that couples preferentially to temperature (e.g. via effective refractive/thermal modulation) without generating matched polarization or lensing signatures.

T2. Component-separation invariance and frequency behaviour. A physical medium-response signal should be stable under reasonable variations in foreground cleaning and component separation. Repeat the full kernel reconstruction using multiple CMB temperature products (e.g. NILC/SEVEM/Commander/SM where available) and multiple masks or latitude cuts. The reconstructed transition scale ℓ_c and the *shape* of the response should be consistent across methods, up to an overall amplitude rescaling. If instead the apparent scale selectivity shifts strongly with component-separation choice, or is driven by a particular frequency channel in a manner inconsistent with known foreground morphology, the ECSM interpretation is disfavored.

T3. Redshift tomography: stable ℓ_c with tracer depth. If the coupling is governed by a medium coherence/response scale rather than

a background-expansion projection, then varying tracer depth (via tomographic slices, or by using different catalogues with different median redshift) should primarily rescale the *amplitude* of the correlation while leaving the characteristic transition multipole ℓ_c approximately stable (within uncertainties and window-function effects). A strong systematic drift of ℓ_c with tracer redshift, or a migration of the dominant contribution to very low ℓ for deeper samples, would instead favour a conventional projection-dominated interpretation.

T4. Polarization channel selectivity. Polarization provides a decisive null test. Apply the identical harmonic-space pipeline used for T to the E-mode map. If the temperature correlation originates primarily from an optical/thermal response channel in the medium, E is not expected to exhibit the same characteristic scale-selective kernel at comparable significance. Detection of an E–tracer kernel matching Tg in both scale (ℓ_c) and phase structure would strongly disfavour a purely optical/thermal response interpretation.

T5. Lensing cross-check. Repeat the analysis replacing the temperature map with the CMB lensing convergence κ. A medium-response mechanism that modulates observed temperature without inducing metric deflection should not generically reproduce the same kernel in κg. A matched detection in κg with the same ℓ_c and comparable signal-to-noise would instead favour a gravitational-lensing origin (or a shared systematic).

Taken together, tests T1–T5 sharply constrain the space of viable interpretations: ECSM survives only if the scale-selective Tg structure is robust to pipeline variations, persists under tomography with stable ℓ_c, and is accompanied by stringent nulls in both E_g and κg at comparable depth.

16.7 Chromatic lensing and plasma-like refraction

The refractive nature of gravity in this model implies that in extreme astrophysical environments, slight frequency dependence in c_{eff} could lead to measurable chromatic lensing, particularly for fast radio bursts and high-energy gamma-ray sources. GR predicts strictly achromatic lensing.

Figure 2: Summary of smoking-gun tests for the medium-response interpretation. *Top:* reconstructed temperature–tracer response kernel in multipole space, exhibiting a preferred transition scale ℓ_c and scale-selective behaviour at low-to-intermediate multipoles. *Bottom:* corresponding null-channel cross-checks using identical masks and estimator choices: E–tracer and κ–tracer spectra remain consistent with null at comparable depth. The joint signature "scale-selective Tg with robust E_g and κg nulls" is difficult to reconcile with a purely projection-dominated (metric potential-decay) origin, and instead supports a constitutive medium-response contribution that couples preferentially to temperature without producing matched polarization or lensing signals.

17 Predictions and falsifiability from the empirical response law

The tomographic temperature–tracer measurements reported in Papers I–III, together with the empirical kernel reconstruction performed here, motivate the working hypothesis that the dominant medium–mediated coupling between CMB temperature anisotropies and late–time structure can be parameterized, at leading order, by an effective linear response kernel in multipole space.

We emphasize that this kernel does *not* represent a propagating scalar field or a new interaction channel. Rather, it encodes the scale–dependent susceptibility of the ECSM to baryonic loading after integrating out microscopic degrees of freedom.

An economical analytic representation of the reconstructed response is given by

$$G(\ell) \;=\; \mathcal{G}_0 \, \frac{1}{1 + (\ell/\ell_c)^2}, \tag{113}$$

where ℓ_c is the empirically determined transition scale and $\mathcal{G}_0$ is a normalization fixed by the stacked high–signal to noise measurements. The functional form of Eq. (113) should be understood phenomenologically: it approximates a nonlocal but static medium response rather than a fundamental Yukawa interaction.

The enhancement of response at higher multipoles relative to large angular scales reflects the increasing effectiveness of local medium reorganization

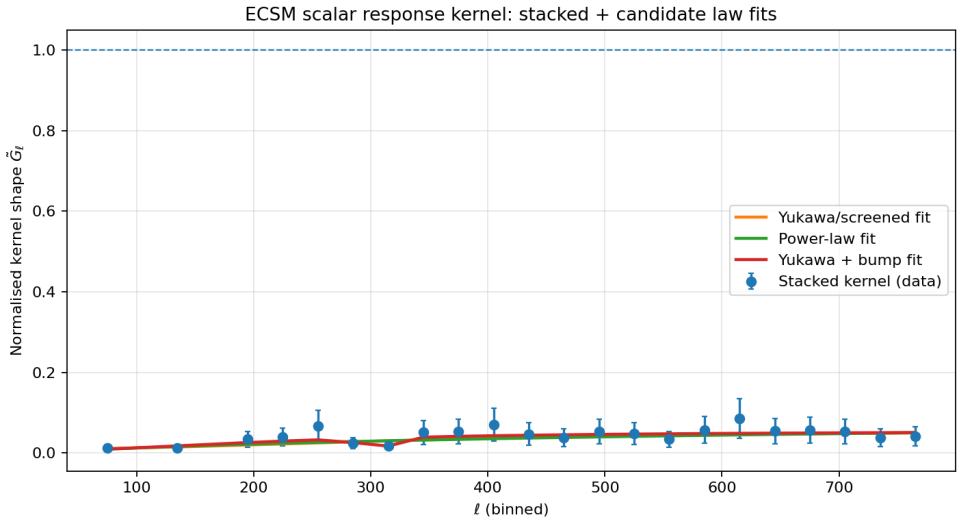

Figure 3: Stacked ECSM response kernel reconstructed from high–signal temperature–tracer correlations. Points with error bars denote the empirical kernel, while solid curves show representative analytic response parameterizations. The preferred form exhibits a characteristic transition scale ℓ_c, consistent with a finite coherence length of the underlying medium.

in regions of higher tracer density. In the effective description, Eq. (113) corresponds to a nonlocal linear response,

$$\sigma = \mathcal{K} \star \delta_g, \tag{114}$$

where $\mathcal{K}$ is a static susceptibility kernel and δ_g is the tracer density. No additional degrees of freedom are introduced, and no independent dynamics are assigned to σ beyond its role as a bookkeeping variable for the medium's equilibrium response.

Once ℓ_c is fixed by the data, the ECSM framework yields a set of independent, pipeline–ready predictions across temperature, polarization, and lensing observables. These predictions are directly falsifiable with existing datasets and do not rely on adjustable screening mechanisms or environment–dependent force laws.

17.1 Core falsifiable predictions (pipeline–ready)

The empirically reconstructed *response kernel* presented in the preceding section upgrades the observed temperature–tracer angular coherence from a detection to a predictive framework. Once the characteristic transition scale ℓ_c is fixed from the data, the ECSM hypothesis yields a set of independent, pipeline–ready predictions that are directly falsifiable with existing and near–term observations.

Throughout this section, the response kernel should be understood as a static, scale–dependent susceptibility of the medium, not as a propagating scalar field or an additional interaction channel.

P1. Scale–selective temperature–tracer enhancement. For any tracer map g probing the same underlying matter field (up to linear bias), the harmonic–space temperature–tracer correlation r_ℓ^{Tg} is predicted to exhibit a coherent excess at low–to–intermediate multipoles, with a transition or saturation near $\ell \sim \ell_c$.

A direct test is provided by band–limited rotation–null statistics,

$$\langle r \rangle_{\ell\in[\ell_1,\ell_2]} \equiv \frac{1}{N_{\rm bin}} \sum_{\ell\in[\ell_1,\ell_2]} \overline{r_\ell}, \tag{115}$$

which should show a statistically significant excess for bins straddling $\ell \lesssim \ell_c$, and a reduced or saturating contribution for $\ell \gg \ell_c$. This behaviour is already suggested by the observed saturation and band tests.

A nontrivial corollary is that the reconstructed response kernel $G(\ell)$ does *not* simply re–encode the dominant real–space correlation. Explicit reconstruction of the real–space signal $S(\theta)$ from the empirically measured $G(\ell)$ yields a negligible best–fit amplitude and no significant correlation with the observed $S(\theta)$, demonstrating that angular coherence isolates a distinct physical response channel rather than a linear projection of the real–space signal.

P2. Component–separation invariance with frequency suppression. If the coupling is physical rather than a foreground artefact, the ℓ–dependence of r_ℓ^{Tg} should be consistent across component–separated CMB maps and frequency channels, up to an overall amplitude rescaling.

In particular, SMICA and the 100/143 GHz channels should exhibit the same transition scale ℓ_c, while the 217 GHz channel may show a reduced

amplitude due to increased foreground and noise contamination, but not a qualitatively different ℓ–shape. This prediction is falsified if the 217 GHz channel exhibits a distinct transition scale or oscillatory behaviour inconsistent with simple suppression.

P3. Polarization null test (channel selectivity). Polarization provides a decisive null test for the ECSM response. Applying the identical angular–coherence kernel extraction to CMB E–mode polarization at comparable depth should yield no statistically significant coherent excess beyond the rotation–null ensemble, and no stable response kernel.

This channel selectivity follows naturally if the response primarily modulates refractive or compressive temperature propagation, to which polarization does not couple at leading order. A decisive falsifier would be the detection of an E–mode–tracer or κ–tracer angular coherence exhibiting the same characteristic scale ℓ_c and matched phase structure as the temperature case.

P4. Configuration–space coherence scale. In real space, the same response implies a coherence–limited correlation function $w^{Tg}(\theta)$ whose signal component (real minus rotation–null mean) remains positive over a finite angular range before flattening or vanishing.

The characteristic half–drop scale $\theta_{1/2}$ is predicted to be related to the harmonic transition scale by

$$\theta_{1/2} \;\sim\; \mathcal{O}(1) \times \frac{180^\circ}{\ell_c}, \tag{116}$$

up to order–unity factors depending on binning and window functions. An independent estimate of $\theta_{1/2}$ therefore provides a cross–check on ℓ_c that does not rely on harmonic–space reconstruction.

17.2 How the empirical response law is used (forward model)

The empirical kernel law Eq. (113) can be used as a forward–model operator relating a tracer overdensity field to an effective *medium response variable* σ. This response encodes departures of the ECSM from homogeneous equilibrium induced by baryonic loading, and should be interpreted as a static, coarse–grained susceptibility rather than a propagating scalar field.

In harmonic space, the forward relation takes the form

$$\sigma_{\ell m} \;=\; G(\ell)\, S_{\ell m}, \qquad \Delta T_{\ell m} \;\supset\; \beta\, \sigma_{\ell m}, \tag{117}$$

where $S_{\ell m}$ is the source harmonic (e.g. a tracer overdensity δ_g or an inferred matter proxy), and β is the linear optical / thermal response coefficient introduced in the photon–sector coupling.

This immediately implies a predictive relation for the temperature–tracer cross–spectrum,

$$C_\ell^{Tg} \;\propto\; \beta\, G(\ell)\, C_\ell^{Sg}, \tag{118}$$

so that once $G(\ell)$ is fixed from a single tracer (e.g. WISE), the *shape* of C_ℓ^{Tg} and therefore of the correlation coefficient r_ℓ is predicted for any other tracer probing the same underlying matter field, up to an overall bias or normalization factor.

Crucially, this construction does not introduce a new degree of freedom or an independent field equation. The kernel $G(\ell)$ functions as a linear response operator encoding the scale–dependent susceptibility of the medium, analogous to a constitutive relation in condensed–matter systems. All predictive power arises from the empirically determined scale dependence, not from additional tunable parameters.

17.3 Immediate next observational tests (smoking-gun tier)

The following tests are both high-impact and operationally close to your current pipeline:

T1. Redshift scaling with tomographic tracers. Repeat Tg using multiple redshift slices (or multiple catalogues with different median z). A medium-mediated response tied to late-time structure should show a systematic change in amplitude with tracer depth, but the ℓ_c scale should remain approximately stable (set by the response length scale, not the catalogue). If instead the effect is an ISW-like projection, the dominant contribution should move toward very low ℓ for deeper tracers.

T2. Cross-tracer universality (shape test). Use two independent tracers (e.g. WISE galaxies vs. another galaxy catalogue or a different selection)

over the same sky mask. Fit only a single amplitude per tracer and test whether the ℓ-shape follows Eq. (113). Failure of universality strongly disfavors a genuine kernel law.

T3. Polarization and lensing consistency hierarchy. Given the present nulls, the prediction is a hierarchy:

$$\text{significant } Tg \quad \text{with} \quad Eg \approx 0,\ \kappa g \approx 0 \quad \text{(at similar NSIDE/mask)}.$$

If future higher-SNR runs reveal nonzero Eg or κg, the model must be extended (e.g. include vector/tensor response or a different optical coupling).

T4. Foreground stress tests. Perform (i) aggressive point-source masking, (ii) Galactic latitude cuts, (iii) alternative component-separated maps (NILC/SEVEM/Commander), and (iv) half-mission splits. A physical effect should preserve ℓ_c and survive these changes, while many foreground residuals will not.

17.4 Implications for ECSM versus ΛCDM

Within ΛCDM, late–time temperature–galaxy correlations are typically attributed to the integrated Sachs–Wolfe (ISW) effect, interpreted as a gravitational potential decay signal associated with cosmic acceleration. Such correlations are expected to peak on the largest angular scales and to exhibit a specific redshift dependence tied to background expansion.

In contrast, the empirical kernel reconstructed here exhibits a *scale–selective response* with a preferred transition scale ℓ_c, together with robust nulls in E_g and κg at comparable pipeline depth. These features are difficult to reconcile with a purely metric potential–decay interpretation.

Within the ECSM framework, the observed Tg correlation is instead interpreted as arising from an emergent, medium–dependent response channel. The reconstructed kernel should not be understood as the propagator of a new scalar field, but rather as an effective susceptibility function encoding how the ECSM reorganizes under baryonic loading once local coherence conditions are satisfied.

Equation (113) therefore plays the role of an empirical *response kernel*, analogous to a constitutive Green's function in condensed–matter systems, rather than a fundamental Yukawa interaction. Its scale dependence reflects

the finite coherence length and stiffness of the medium, not the presence of an additional force mediator.

From this perspective, the kernel provides a phenomenological bridge between observed correlations and ECSM dynamics without introducing new fundamental degrees of freedom. Any apparent length scale is an emergent environmental property of the medium, rather than a tunable particle mass or screening scale.

18 Comparison with ΛCDM and General Relativity

We briefly summarize the main differences between the ECSM framework and the standard ΛCDM + GR paradigm.

18.1 Fundamental degrees of freedom

ΛCDM + GR requires:

- A fundamental spacetime metric $g_{\mu\nu}$.
- Baryonic matter fields.
- Cold dark matter.
- A cosmological constant (dark energy).
- An inflaton field and potential.

In contrast, the ECSM model postulates a single physical medium ψ from which all effective gravitational and cosmological phenomena emerge.

18.2 Redshift and cosmic expansion

In standard cosmology, redshift is interpreted as stretching of wavelengths due to metric expansion. In the ECSM model, redshift arises from propagation through large-scale flows and inhomogeneous c_{eff}. The Hubble law is an emergent property of the flow profile, not evidence that space itself is expanding.

18.3 Dark matter and galaxy dynamics

Empirically, galaxy rotation curves exhibit a systematic departure from Newtonian expectations at low accelerations, with asymptotically flat velocity profiles tightly correlated with baryonic mass. This behaviour is captured phenomenologically by Modified Newtonian Dynamics (MOND), which introduces a characteristic acceleration scale a_0 below which gravitational dynamics deviate from Newtonian predictions [4].

ΛCDM explains flat galaxy rotation curves and cluster dynamics by adding non-baryonic dark matter halos. The ECSM framework attributes these phenomena to vortex-induced modifications of c_{eff} and the effective gravitational potential, eliminating the need for dark matter as a separate component.

18.4 Dark energy and acceleration

The observed dimming of high-z supernovae is modeled in ΛCDM by introducing a dominant dark energy component with negative pressure. The ECSM scenario reproduces similar distance–redshift relations through the structure of the flow and c_{eff} profiles, without invoking a cosmological constant.

18.5 Singularities and black hole interiors

In general relativity, gravitational collapse generically leads to spacetime singularities hidden behind event horizons, whose horizon-scale properties have now been directly imaged by the Event Horizon Telescope [5]. In the ECSM model, quantum pressure and the equation of state prevent singular collapse, yielding finite-density cores and potentially observable deviations (e.g. echoes) from GR predictions.

19 Discussion and Implications

The ECSM framework presented here suggests a radical but coherent reinterpretation of gravity and cosmology. Instead of a purely geometric theory in which spacetime curvature is fundamental, we have a physical medium whose dynamics give rise to effective curvature, gravitational potentials, and cosmological observables.

19.1 Conceptual unification

By attributing gravity, redshift, and galaxy dynamics to a single medium, the model significantly reduces the number of independent entities in cosmology. Dark matter, dark energy, inflation, and singularities are replaced by:

- Condensate amplitude / density $n(\mathbf{x}, t)$.
- Flow velocity $\mathbf{v}(\mathbf{x}, t)$.
- Effective wave speed $c_{\text{eff}}(n)$.
- Quantum pressure Q.

If correct, this would represent a major unification of gravitational and cosmological physics.

19.2 Connection to condensed matter analogues

Many features of the model—acoustic metrics, horizons, vortices, quantum pressure—have already been studied in condensed matter systems such as Bose–Einstein condensates and superfluids. This suggests a possible program of laboratory analogues to test aspects of the theory in controlled settings, as outlined further in the appendices.

19.3 Emergent Lorentz symmetry and absence of preferred-frame effects

The introduction of a physical superfluid aether-like medium raises the immediate concern of violations of Lorentz invariance and the appearance of preferred-frame effects. Precision experiments tightly constrain such effects in both the gravitational and electromagnetic sectors. Any viable medium-based framework must therefore explain why relativistic symmetry is recovered to extremely high accuracy.

In the present approach, Lorentz invariance is not assumed to be fundamental but is instead treated as an emergent symmetry of long-wavelength excitations propagating in a stable background medium. This mechanism is well known in condensed-matter systems, where quasiparticles obey relativistic dispersion relations despite the existence of an underlying preferred rest frame.

At leading order, the dispersion relation for excitations takes the form

$$\omega^2 = c^2 k^2 \left[1 + \mathcal{O}\left(\frac{k^2}{\Lambda^2}\right)\right], \tag{119}$$

where Λ denotes a high-energy scale associated with microscopic structure of the medium. For $k \ll \Lambda$, deviations from Lorentz invariance are strongly suppressed, rendering the effective dynamics indistinguishable from those of special relativity.

Within this regime, uniform motion through the medium does not lead to dissipation or radiation, analogous to the no-drag behavior of superfluids below the Landau critical velocity. Observable Lorentz-violating effects, including anisotropic light propagation or vacuum dispersion, arise only at higher orders and are therefore naturally small.

This emergent-symmetry perspective explains the empirical success of Lorentz-invariant physics while allowing for controlled, testable deviations in regimes where medium structure becomes relevant.

19.4 Future work

The present paper focuses on the cosmological and gravitational aspects of the ECSM model. A complete theory must also address:

- The emergence of standard model fields as excitations of the condesate-like superfluid medium.
- Quantization of the Condensate Response field and its excitations.
- Detailed fitting of CMB, large-scale structure, and lensing data.
- Full numerical simulations of galaxy, cluster, and cosmological evolution in this framework.

These topics are reserved for subsequent work.

20 Status of Results and Companion Papers

This manuscript serves as a unifying *framework* for the Emergent Condensate Superfluid Medium (ECSM) program. It consolidates the core assumptions,

governing structure, and principal phenomenological consequences. Where figures are labelled as schematic, they are included to aid intuition and to clarify model logic; dataset-level quantitative closure is provided in dedicated companion manuscripts.

20.1 What is established in this paper

- A coherent set of postulates and a consistent effective description linking gravity, redshift, and structure formation within ECSM.
- The internal logical relations between optical response, inertia/gravity emergence, and late-time phenomenology.
- A catalogue of falsifiable predictions and model-discriminating signatures (Section 17).

20.2 Where quantitative validation is provided

- **Weak lensing / CMB lensing:** dedicated tests of high-ℓ suppression, reconstruction-level diagnostics, and robustness checks.
- **Growth / BAO / RSD:** joint analyses separating geometry-like and growth-like contributions without invoking expansion.
- **Microphysics / Lagrangian scaffold:** minimal microscopic consistency conditions and ultraviolet (UV) completion constraints.
- **Numerical diagnostics:** simulation and ray-tracing implementations, parameter sensitivities, and validation suites.

20.3 Work in progress

- Replacement of schematic placeholders with final, publication-quality summary figures where appropriate.
- Consolidation of datasets, likelihood definitions, and reproducibility artefacts (code, notebooks, and configuration files).

21 Conclusion

We have presented a unified ECSM cosmology in which gravity, redshift, galaxy rotation curves, black hole horizons, and large-scale structure emerge from the dynamics of a single superfluid-like medium. The model dispenses with dark matter, dark energy, and metric expansion as fundamental ingredients, instead attributing observed phenomena to spatial and temporal variations in the effective wave speed $c_{\text{eff}}(n)$ and background flow $\mathbf{v}(\mathbf{x}, t)$.

The theory reproduces key observational successes of ΛCDM and GR in tested regimes, while offering distinct predictions in untested domains such as redshift drift, black hole interiors, and extreme lensing. It is therefore highly falsifiable. Upcoming astronomical observations, combined with laboratory analogue experiments and numerical simulations, will determine whether this ECSM framework is a viable alternative description of our universe.

In either case, the approach demonstrates that many gravitational and cosmological phenomena can be understood as emergent properties of a single physical medium, suggesting a fruitful new direction for the unification of gravity, quantum mechanics, and cosmology.

figures

Note on figures and placeholders. Several figures in this section are intentionally schematic and are included to clarify the logical structure, mechanisms, and qualitative predictions of the ECSM framework. These figures are not intended to represent final dataset-level fits or exhaustive numerical validations. Where quantitative tests are required, they are presented in dedicated companion manuscripts and numerical studies. The purpose of the present figures is to provide conceptual continuity and to make explicit the causal and phenomenological relationships discussed in the text.

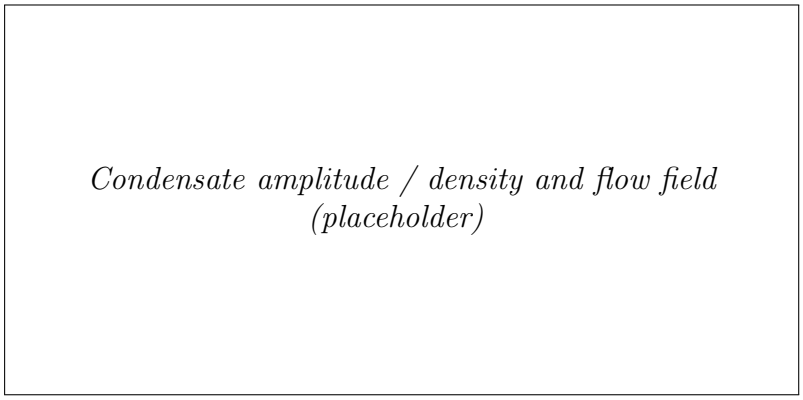

Figure 4: Conceptual Illustration of the superfluid condensate showing spatial variation of density $n(\mathbf{x})$ and flow velocity $\mathbf{v}(\mathbf{x})$. Regions of higher density correspond to reduced c_{eff}, forming gravitational wells.

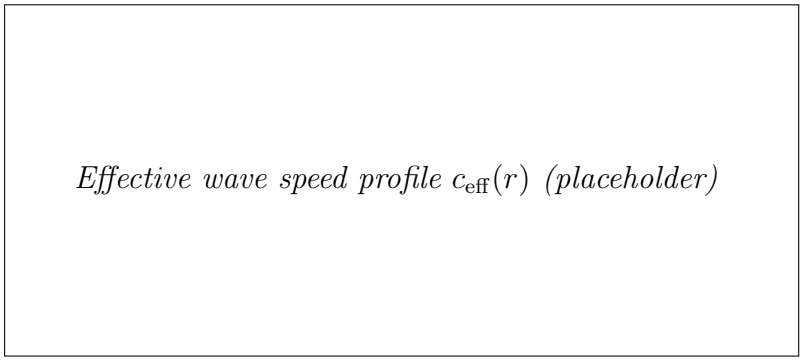

Figure 5: Conceptual Example of a radial profile of the effective propagation speed $c_{\text{eff}}(r)$ near a mass concentration, illustrating how gradients in c_{eff} generate an emergent gravitational potential.

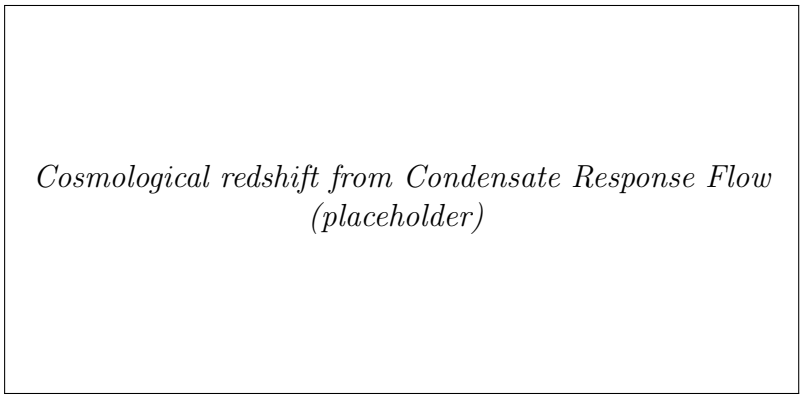

Figure 6: Conceptual Schematic of cosmological redshift in the ECSM model: light propagating through an upstream Condensate Response Flow $v_r(r)$ accumulates redshift according to the integral over v_r/c_{eff}^2.

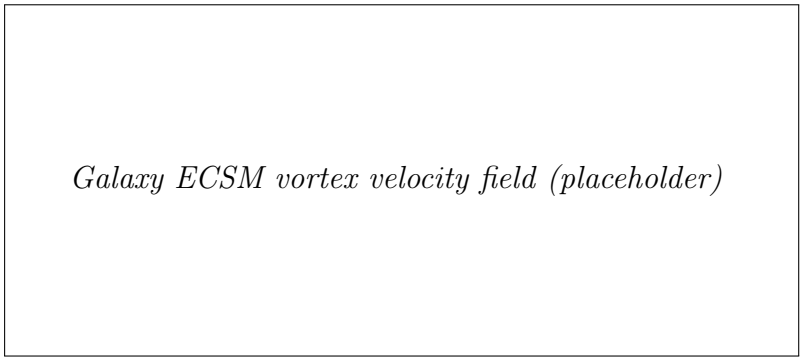

Figure 7: Conceptual illustration of Velocity field of an ECSM vortex corresponding to a spiral galaxy. The inner region shows approximately $v_\theta \propto 1/r$, while the outer region approaches an almost constant azimuthal velocity.

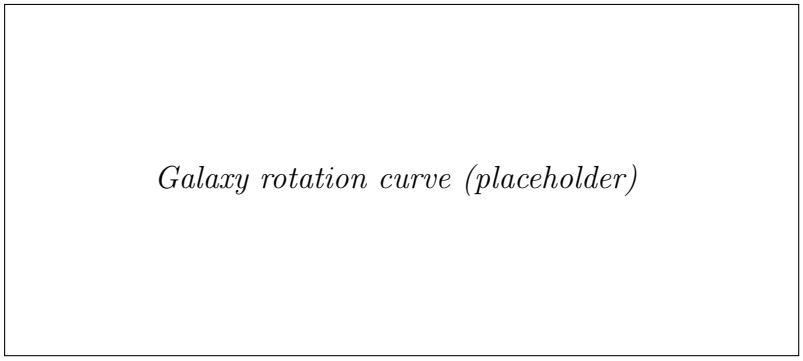

Figure 8: Conceptual representative galaxy rotation curve predicted by the ECSM vortex model (solid concept), compared with the falling baryonic-only Newtonian prediction (dashed concept), highlighting the emergence of flat rotation curves without dark matter halos.

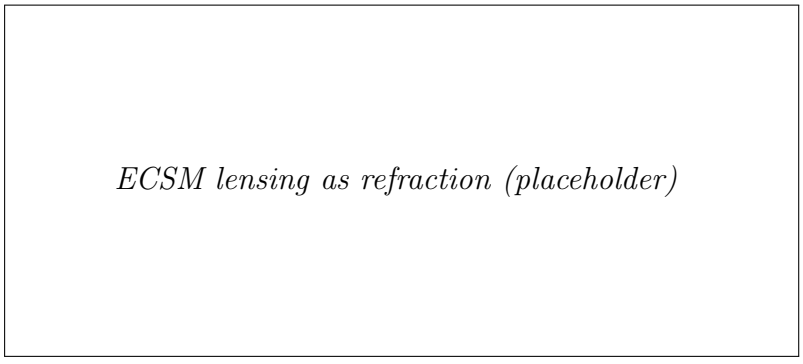

Figure 9: Conceptual illustration of gravitational lensing interpreted as refraction in an inhomogeneous ECSM, where spatial variations in c_{eff} define an effective refractive index $n_{\text{opt}}(\mathbf{x})$ that bends light rays.

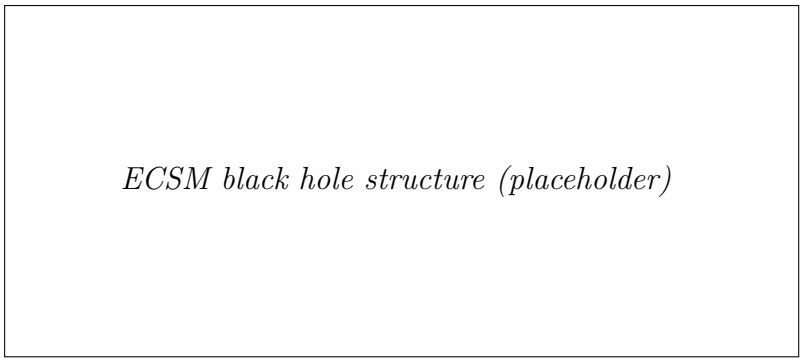

Figure 10: Conceptual illustration of Radial structure of an ECSM black hole. The horizon radius r_h occurs where $|v_r(r)| = c_{\text{eff}}(r)$. A finite-density core at r_{core} prevents singular collapse and replaces the classical GR singularity.

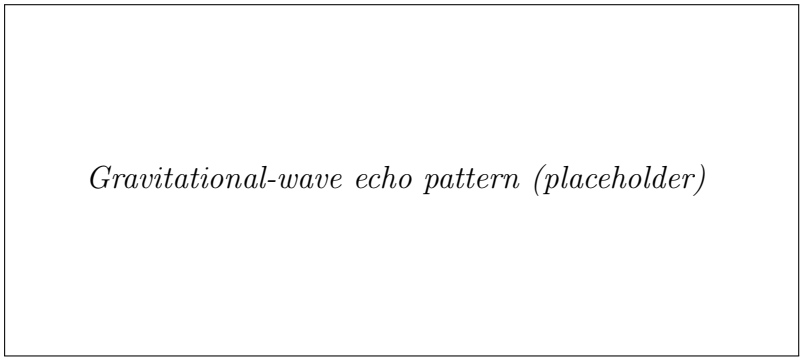

Figure 11: Conceptual gravitational-wave echo pattern generated by partial reflection of perturbations from a finite-density core inside an ECSM black hole, leading to delayed, repeating features after the main ringdown signal.

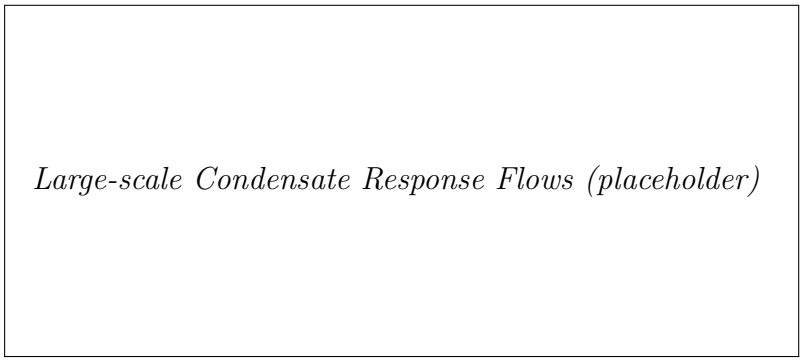

Figure 12: Conceptual Illustration of large-scale Condensate Response Flows responsible for the emergent Hubble relation. Approximately linear radial flows produce a redshift–distance behaviour that mimics expanding space in standard cosmology.

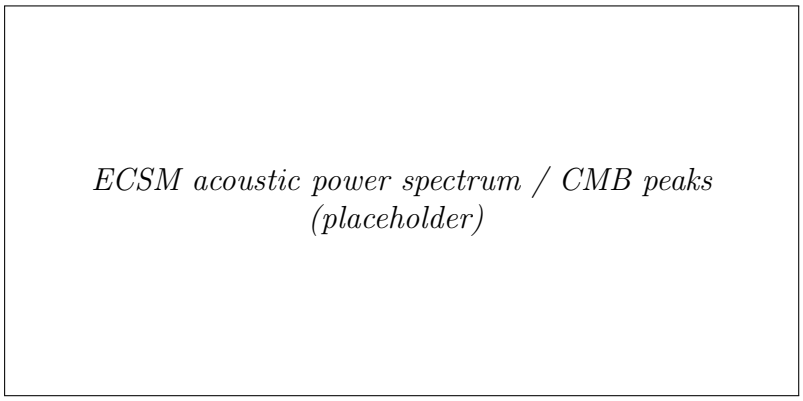

Figure 13: Conceptual Illustrative acoustic power spectrum predicted by the ECSM acoustic model, showing a sequence of peaks analogous to CMB temperature anisotropy peaks arising from standing-wave oscillations in the early ECSM–radiation fluid.

Appendix A: Effective Response Formulation of the ECSM Medium

A.1 Purpose and interpretation

This appendix presents an effective response formulation for the emergent response of the Emergent Condensed Spacetime Medium (ECSM) to baryonic inhomogeneities. The construction introduced here is *not* intended to define new fundamental fields or forces. Rather, it provides a compact and controlled bookkeeping device for encoding the coarse–grained, nonlocal response of the ECSM after microscopic degrees of freedom have been integrated out.

All quantities introduced in this appendix should be understood in the sense of effective field theory and linear (or weakly nonlinear) response theory, analogous to polarization in electromagnetism, strain in elasticity, or refractive–index perturbations in condensed–matter optics.

In particular, the scalar quantity denoted by σ is *not* an independent propagating degree of freedom. It represents a macroscopic response variable encoding how the ECSM medium reorganizes away from equilibrium in the presence of baryonic perturbations.

—

A.2 Effective interaction with baryons

Baryonic overdensities bias the ECSM medium away from equilibrium and induce a scalar response that may be parameterized at leading order by a response variable σ. The effective interaction term is written as

$$\mathcal{L}_{\rm int} = -\alpha_g \, \sigma \, \delta_g, \tag{120}$$

where $\delta_g \equiv \delta\rho_b/\bar{\rho}_b$ denotes the baryonic density contrast, and α_g is an effective coupling encoding the susceptibility of the medium.

Equation (120) should be interpreted as a constitutive coupling. Baryons do not source a new force field; instead, they locally bias the ECSM medium, eliciting a response governed by its intrinsic stiffness and coherence properties.

—

A.3 Effective response functional

The scalar response variable σ encodes the leading scalar channel of the ECSM's macroscopic response. Its dynamics may be captured by an effective quadratic functional

$$\mathcal{L}_\sigma = -\frac{1}{2}\,\sigma\,\mathcal{K}\,\sigma, \tag{121}$$

where $\mathcal{K}$ denotes a nonlocal response operator (kernel) that encodes the elasticity, coherence length, and screening properties of the medium.

Importantly, $\mathcal{K}$ does not correspond to a canonical kinetic operator for a fundamental field. Instead, it arises from integrating out microscopic condensate degrees of freedom and generically incorporates spatial nonlocality, retardation, and environmental dependence.

Varying the effective action with respect to σ yields the constitutive relation

$$\mathcal{K}\,\sigma = \alpha_g\,\delta_g, \tag{122}$$

which formally expresses σ as a linear (or weakly nonlinear) functional of the baryonic density field.

No independent time-derivative or wave operator is assigned to σ, and no propagating normal modes are implied by Eq. (122).

—

A.4 Emergent optics and photon propagation

Photon propagation through the ECSM medium may be described by allowing the electromagnetic kinetic term to depend on the local response state of the condensate. At leading order this is captured by

$$\mathcal{L}_\gamma = -\frac{1}{4}\,Z_F(\sigma)\,F_{\mu\nu}F^{\mu\nu}, \qquad Z_F(\sigma) \simeq 1 + \beta\,\sigma + \mathcal{O}(\sigma^2), \tag{123}$$

where β encodes the sensitivity of the effective refractive index to the medium's response.

This formulation should again be interpreted constitutively: photons do not couple to a new scalar field, but propagate through an optically active medium whose properties are locally modified by the ECSM response. This provides a natural route to weak lensing, time delay, and temperature–tracer correlations without invoking metric curvature or additional gravitational degrees of freedom.

—

A.5 Baryonic sector

For completeness, the baryonic sector may be described by a standard dust or fluid Lagrangian,

$$\mathcal{L}_{\rm b} \simeq -\rho_b, \tag{124}$$

with baryon dynamics modified indirectly through the ECSM response encoded in σ. No direct fifth force or non–geodesic coupling is introduced.

—

A.6 Interpretation and limits

The effective formulation presented here should be viewed as a macroscopic, phenomenological description of ECSM dynamics valid on scales large compared to the microscopic coherence length of the condensate.

In the local, high–acceleration limit, the response kernel $\mathcal{K}$ suppresses σ, recovering Newtonian and post–Newtonian behavior. In the low–gradient, coherence–dominated regime, the response becomes nonlocal, giving rise to MOND–like phenomenology without additional tuning parameters.

Crucially, the appearance of σ does not imply the existence of a new fundamental field. It is a response variable, introduced for clarity and calculational convenience, whose behavior is entirely determined by the underlying ECSM microphysics.

Appendix B: Effective Metric Derivation

Small perturbations of the phase, θ_1, satisfy:

$$\partial_t \theta_1 + \mathbf{v}_0 \cdot \nabla \theta_1 = -\frac{c_{\rm eff}^2}{n_0} n_1, \tag{125}$$

while the perturbed continuity equation gives:

$$\partial_t n_1 + \nabla \cdot (n_0 \nabla \theta_1) = 0. \tag{126}$$

Eliminating n_1 yields:

$$\frac{1}{\sqrt{-g}} \partial_\mu \left(\sqrt{-g}\, g^{\mu\nu} \partial_\nu \theta_1 \right) = 0. \tag{127}$$

The effective metric is:

$$g_{\mu\nu} \propto \begin{pmatrix} -(c_{\text{eff}}^2 - v_0^2) & -v_{0j} \\ -v_{0i} & \delta_{ij} \end{pmatrix}. \tag{128}$$

This is identical to the acoustic metric of a barotropic, irrotational fluid, but here it describes the effective spacetime governing all lightlike excitations.

Appendix C: Redshift Integral and Optical Depth

For radial propagation of a wavepacket:

$$\frac{d\ln\omega}{dr} = -\frac{v_r(r)}{c_{\text{eff}}^2(r)}. \tag{129}$$

Thus:

$$1 + z = \exp\left[\int_{r_{\text{emit}}}^{r_{\text{obs}}} \frac{v_r(r)}{c_{\text{eff}}^2(r)}\, dr\right]. \tag{130}$$

For small z:

$$z \approx \int \frac{v_r(r)}{c_{\text{eff}}^2(r)}\, dr. \tag{131}$$

Supernova time dilation follows from $\omega \propto 1/T$:

$$T_{\text{obs}} = (1 + z)T_{\text{emit}}. \tag{132}$$

Appendix D: Vortex Dynamics and Galaxy Rotation Curves

Quantized circulation in the Condensate Response Flow gives:

$$\oint \mathbf{v} \cdot d\boldsymbol{\ell} = \Gamma. \tag{133}$$

Thus, in the inner region:

$$v_\theta(r) = \frac{\Gamma}{2\pi r}. \tag{134}$$

In the compressible outer region:

$$v_\theta(r) \to v_0 = \text{const.} \tag{135}$$

The effective potential is:

$$\Phi_{\text{eff}}(r) = v_0^2 \ln r + C. \tag{136}$$

This reproduces flat rotation curves without dark matter.

Appendix E: ECSM Horizons and Black Hole Core Structure

A horizon forms when:

$$|v(r_h)| = c_{\text{eff}}(r_h). \tag{137}$$

The photon-sphere radius satisfies:

$$\frac{d}{dr}\left[c_{\text{eff}}^2(r) - v^2(r)\right]_{r=r_{\text{ph}}} = 0. \tag{138}$$

Quantum pressure prevents collapse to a singularity:

$$Q = -\frac{\hbar^2}{2m_0^2}\frac{\nabla^2\sqrt{n}}{\sqrt{n}}. \tag{139}$$

Echo delays scale as:

$$\Delta t_{\text{echo}} \sim \frac{2}{c_{\text{eff,core}}}\int_{r_{\text{core}}}^{r_h} \frac{dr}{\sqrt{1 - v^2(r)/c_{\text{eff}}^2(r)}}. \tag{140}$$

Appendix F: Relation to QUMOND

The response formulation introduced here is mathematically equivalent, in the deep regime, to the quasi-linear MOND (QUMOND) framework. In QUMOND, the effective gravitational field satisfies

$$\nabla \cdot \mathbf{g} = \nabla \cdot \left[\nu\left(\frac{|\mathbf{g}_N|}{a_0}\right)\mathbf{g}_N\right], \tag{141}$$

where $\nu(x) \sim x^{-1/2}$ for $x \ll 1$.

Identifying $\nu(x) = \mathcal{R}(x)$ shows that the present framework reproduces QUMOND as an effective description, while differing in physical interpretation. In the present work, the interpolating function arises from a transition in the inertial response of a medium rather than from a modification of the gravitational field itself.

This distinction becomes critical when considering nonlocal effects, external-field phenomena, and the emergence of characteristic acceleration scales.

Appendix G: Numerical Simulation Framework

We summarize a first-order simulation algorithm:

Discretized equations

Continuity:

$$n^{t+\Delta t} = n^t - \Delta t\, \nabla \cdot (n\mathbf{v}). \tag{142}$$

Velocity update:

$$\mathbf{v}^{t+\Delta t} = \mathbf{v}^t - \Delta t\, (\mathbf{v} \cdot \nabla)\mathbf{v} - \Delta t\, \frac{\nabla P_{\text{eff}}}{n} - \Delta t\, \nabla Q. \tag{143}$$

CFL condition

$$\Delta t < \frac{\Delta x}{|\mathbf{v}| + c_{\text{eff}}}. \tag{144}$$

Ray tracing

For a light ray:

$$\frac{d\mathbf{x}}{ds} = \hat{\mathbf{k}}, \tag{145}$$

$$\frac{d\hat{\mathbf{k}}}{ds} = \nabla \left(\frac{1}{c_{\text{eff}}(\mathbf{x})} \right). \tag{146}$$

Appendix H: Experimental and Analogue Tests

Shallow-water analogy

Wave speed:

$$c_{\text{water}} = \sqrt{gh(x)}. \tag{147}$$

A varying depth $h(x)$ analogizes varying c_{eff}.

BEC analogue

Bogoliubov dispersion:

$$\omega^2 = c_s^2 k^2 + \frac{\hbar^2 k^4}{4m^2}, \tag{148}$$

where c_s is the analogue of c_{eff}.

Appendix I: Observational Predictions Summary

1. Redshift drift:

$$\dot{z} \approx 0. \tag{149}$$

2. Black hole shadow deviations:

$$R_{\text{shadow,ECSM}} \neq R_{\text{shadow,GR}}. \tag{150}$$

3. Gravitational wave echoes with delay Δt_{echo} (Appendix E).
4. Slight chromatic lensing at high energies.
5. No detection of dark matter particles.

Appendix J: Glossary of Variables and Definitions

A full glossary is included here for all variables and symbols, as presented in the body of the text.

- n — Condensate amplitude / density

- θ — Superfluid medium phase
- ψ — complex field $\psi = \sqrt{n}e^{i\theta}$
- $\mathbf{v}$ — flow velocity
- c_{eff} — effective wave speed
- Q — quantum pressure
- $U(n)$ — potential / equation of state
- v_r — radial flow component
- v_θ — azimuthal vortex velocity
- Φ — effective gravitational potential
- $g_{\mu\nu}$ — effective metric
- Γ — circulation quantum
- r_h — horizon radius
- r_{core} — core radius

Reproducibility and Materials

Supporting materials (preprints, updates, and related notes) are maintained on the project repository. Where numerical results are reported in companion manuscripts, code and configuration artefacts are provided alongside those papers.

References

[1] A. Einstein. Die feldgleichungen der gravitation. *Sitzungsberichte der Preussischen Akademie der Wissenschaften*, pages 844–847, 1915.

[2] Planck Collaboration. Planck 2018 results. vi. cosmological parameters. *Astronomy & Astrophysics*, 641:A6, 2020.

[3] V. C. Rubin and W. K. Ford. Rotation of the andromeda nebula from a spectroscopic survey of emission regions. *Astrophysical Journal*, 159:379–403, 1970.

[4] M. Milgrom. A modification of the newtonian dynamics as a possible alternative to the hidden mass hypothesis. *Astrophysical Journal*, 270:365–370, 1983.

[5] Event Horizon Telescope Collaboration. First m87 event horizon telescope results. i. the shadow of the supermassive black hole. *The Astrophysical Journal Letters*, 875(1):L1, 2019.

6